4' SST Section Copy No. 1

NATIONAL ADVISORY COMMITTEE FOR AERONAUTICS

TECHNICAL NOTE

No. 1642

VELOCITY DISTRIBUTIONS ON SYMMETRICAL AIRFOILS IN CLOSED TUNNELS BY CONFORMAL MAPPING

By W. Perl and H. E. Moses

Flight Propulsion Research Laboratory
Cleveland, Ohio

Washington
June 1948

ERRATA

NACA TN No. 1642

VELOCITY DISTRIBUTIONS ON SYMMETRICAL AIRFOILS IN CLOSED TUNNELS BY CONFORMAL MAPPING

By W. Perl and H. E. Moses

Page 16, line 6 after equation (B5): Omit parenthetical expression ($\epsilon = \varphi - \theta$).

NATIONAL ADVISORY COMMITTEE FOR AERONAUTICS

TECHNICAL NOTE NO. 1642

VELOCITY DISTRIBUTIONS ON SYMMETRICAL AIRFOILS IN CLOSED TUNNELS BY CONFORMAL MAPPING

By W. Perl and H. E. Moses

SUMMARY

Conformal-mapping methods recently developed are applied to the calculation of the constraining effect of the tunnel walls on the ideal zero-lift flow past arbitrary symmetrical airfoils. The results are compared with those of the conventional first-order image theory, of Goldstein's second-order image theory, and of a stream-filament theory with approximate allowance made for the curvature of the streamlines. The local constriction corrections obtained by the Goldstein second-order image theory agree with those calculated by conformal mapping better than those calculated by first-order image theory.

INTRODUCTION

When a body is investigated in a closed wind tunnel, the effect of the walls is to constrain the flow past the body and to modify its free-stream pressure distribution. Recent tendencies to test models of large size relative to the tunnel have resulted in large constriction effects, of which the accuracy of determination by first-order image theory is doubtful or inadequate; consequently, a more detailed investigation of this effect was undertaken at the NACA Cleveland laboratory because of its immediate connection with work conducted in the Cleveland altitude wind tunnel.

The phase of the problem reported in this paper is the case where the flow is two-dimensional, nonviscous, and incompressible and the airfoil is symmetrical and symmetrically located between the walls of the two-dimensional tunnel. The scope of the investigation included calculation of the velocity distributions on an airfoil 12 percent and 24 percent thick at ratios of airfoil chord to tunnel height of 0.5, 1.0, 1.5, 2.0, and 0 (the isolated airfoil case).

The conformal-mapping methods of references 1 and 2, suitably adapted and extended, were used in the study and are briefly outlined.

before the presentation of the results. Results were obtained to a high degree of exactitude in order that a rigorous comparison with other methods could be made. Comparison was made with the results obtained by three other theories: (1) the simple image theory summarized for Glauert in reference 3, (2) the more thoroughgoing image theory recently put forth by Goldstein in reference 4, and (3) an elementary stream-filament theory. In the simple image theory, the airfoil is assumed to be small in thickness t and chord c relative to the tunnel height h. The resulting constriction correction, defined as the difference between the tunnel and the isolated-airfoil nondimensional airfoil velocity distributions, is correct to the order tc/h^2. The image theory of Goldstein is, in principle, capable of yielding results correct to any order. The successive approximations required become so increasingly laborious, however, that Goldstein gives formulas for the constriction correction valid only to the next higher orders; namely, tc^3/h^4, t^2c^2/h^4, t^3c/h^4. In the stream-filament theory, a simple assumption as to the magnitude of the curvature of the flow streamlines permitted integration of the irrotational condition and subsequent determination of the function of integration by the continuity condition.

The stream-filament method was developed primarily to check the results obtained by conformal mapping at the higher values of c/h. The method is interesting in its own right, however, and appears likely to be useful in more general flow problems.

SYMBOLS

The following symbols are used herein:

c chord of airfoil

c/h ratio of chord of airfoil to height of tunnel (solidity)

h height of tunnel

t maximum thickness of airfoil

t/c thickness ratio of airfoil

V undisturbed stream velocity

v_c velocity on airfoil in tunnel or equivalent cascade

v_i velocity on airfoil in free stream (isolated airfoil)

$\Delta v/V$ constriction correction, $v_c/V - v_i/V$

z point in physical plane $(x + iy)$

ζ point in mapping plane of airfoil chord $(\xi + iy)$

Δx horizontal displacement between conformally corresponding points

Δy vertical displacement between conformally corresponding points

METHOD OF CONFORMAL MAPPING

As is well known (reference 3, p. 52), the potential flow about a symmetrical airfoil symmetrically located in a closed two-dimensional tunnel is identical with the symmetrical flow through the unstaggered cascade of airfoils that arises from the imaging of the airfoil successively in the tunnel walls. (See fig. 1.) The evaluation of the tunnel-constriction correction is therefore reduced to a comparison of the velocity distributions of the airfoil in symmetrical cascade flow and in symmetrical isolated flow.

The first method of conformal mapping used to obtain the symmetrical cascade flow was a straightforward adaptation of the method of reference 2. For the isolated-airfoil case, the airfoil contour was mapped into a straight-line contour and the straight line taken as the extended chord line of the airfoil (line AB, fig. 1). The function that accomplishes the mapping is the vector distance $z-\zeta$ between conformally corresponding points of the two contours and has been called the Cartesian mapping function or CMF. (See reference 1.) The imaginary part Δy of the CMF consists of the given ordinates of the airfoil measured from the chord line. The real part Δx is calculated from the imaginary part by a well-known mathematical operation, which thereby determines the mapping function. The velocity distribution is determined by the mapping function and the known (uniform) flow past the straight-line contour. In the cascade case, a slight algebraic alteration in the procedure is required, which corresponds to the fact that the airfoil and the straight line, instead of being isolated, are each one of a cascade of airfoils and straight lines, respectively.

It was found in applying this method (referred to as "the method of finite chord") that for solidities $c/h > 1$ the standard set of chordwise stations on the airfoil, at which the velocities were being calculated, crowded inordinately toward the center of the airfoil.

Some uncertainty and insufficient detail in the results toward the airfoil extremities were thereby obtained, as will be shown later. In order to remedy this deficiency, a variation of the basic method was resorted to, which is referred to as "the method of semi-infinite chord." The given contour to be transformed into a straight line was taken, not as the airfoil itself, but as the airfoil together with the infinite straight-line prolongation CD in figure 1. The chord-line contour into which this contour is to be transformed is line ED in figure 1. The effect of mapping these two contours is to make possible a choice of distribution of the standard set of chordwise stations on the upstream half of the airfoil. A suitable distribution of the standard set of chordwise locations on the downstream half of the airfoil was obtained by mapping the airfoil and its infinite straight-line prolongation in the other direction EF into the infinite chord line CF.

The method of finite chord was finally used for solidities of 0 and 0.5 and the method of semi-infinite chord was used for solidities of 1.0, 1.5, and 2.0.

Details of these mapping methods are given in appendixes A, B, and C. The details of the simple image method, the Goldstein image method, and the stream-filament method are given in appendixes D, E, and F, respectively.

RESULTS

The 12-percent- and 24-percent-thick airfoils for which calculations were made are shown in figure 2. The airfoil ordinates are listed in table I. Shown in figure 2 is the Kaplan section (reference 5) for which some calculations were also made.

Listed in tables II to X and plotted in figures 3 to 8 are the following results:

1. Obtained by conformal mapping:

   (a) Velocity distributions for solidities of 0, 0.5, 1.0, 1.5, and 2.0 (fig. 3, tables II and III).

   (b) Local constriction corrections: difference between tunnel and isolated-airfoil velocity distributions (figs. 4 and 5, tables IV and V; note different ordinate scale in figs. 5(c) and 5(d)).

(c) Average constriction corrections: chordwise average of local constriction correction from 10-percent to 90-percent chord plotted against tc/h^2 for 12- and 24-percent-thick airfoils (fig. 6, table VI).

488

2. Obtained by simple image and Goldstein image theories:

(a) Local constriction corrections using isolated-airfoil velocity distributions obtained by conformal mapping (figs. 4 and 5, tables IV and V).

(b) Average constriction correction, obtained as described in 1(c) (fig. 6, table VI).

3. Obtained by stream-filament theory: Velocity distributions obtained for solidities of 1.0, 1.5, and 2.0 for 12-percent- and 24-percent-thick airfoils (fig. 3).

4. Average constriction corrections obtained by conformal-mapping method for 12- and 24-percent-thick airfoils and 10-percent Kaplan section:

(a) Plotted against tc/h^2 (fig. 7(a)).

(b) Plotted against c/h (fig. 7(b)).

(c) Plotted against t/h (fig. 7(c)).

5. Conformal-mapping data for the various airfoils (tables II, III, VII, and VIII).

6. Comparison of the two conformal-mapping methods (fig. 8).

7. Critical Mach numbers of isolated airfoils calculated by the various correction methods (table IX).

8. Constants occurring in first- and second-order image theories (table X).

DISCUSSION AND COMPARISON

Accuracy

In the methods of conformal mapping, a sufficient number of successive approximations were made (three or four) so that coincidence of the derived airfoil with the given airfoil (appendix A) was achieved to a scale of 20 inches for the length of the chord and the ordinate scale five times the abscissa scale. In order to give some idea of the accuracy of the solutions obtained, the individual chordwise locations at which velocities were obtained are shown in figure 8 for a typical case, namely, 12-percent-thick airfoil and $c/h = 1.5$. By the method of finite chord, 11 chordwise locations were obtained over the middle portion of the airfoil and, by the method of semi-infinite chord, 23 chordwise locations each over approximately the leading half and the trailing half of the airfoil. Aside from the tailed points, which are inherently least accurate in the method of semi-infinite chord, the results obtained by this method overlap each other at the center and also closely agree with the results of the method of finite chord. The consistency of the velocity distributions in the severest case calculated, namely, 24-percent-thick airfoil and $c/h = 2.0$, is estimated from a comparison of the different conformal-mapping methods to be within 0.5 percent. Absolute accuracy of the results is therefore probably of this order. The local constriction corrections are hence believed to be no more than 2 percent in error.

Velocity Distributions

The velocity distributions of the 12-percent- and 24-percent-thick airfoils (fig. 3) show the same general character at high solidity as at low solidity. The peak velocity increases with solidity at a greater rate than the velocity elsewhere on the airfoil. At the higher solidities local irregularities appear in the velocity distributions that are not apparent at the low solidities. These irregularities have been traced to corresponding irregularities in the curvature of the airfoil by means of the stream-filament theory, in which local fluctuations of velocity are a direct consequence of curvature fluctuations on the airfoil surface at the same chordwise locations. (See appendix F.) The velocity distributions obtained by the stream-filament method are indicated in figure 3. Agreement with the velocity distributions by conformal mapping is excellent at a solidity of 2.0 and, as is to be expected, the agreement falls off with decrease in solidity. Considering the simplicity of the method, the stream-filament theory gives surprisingly good results and merits further investigation. The velocity fluctuations in figure 3 illustrate the importance of designing boundary surfaces to have smooth curvature distributions, if smooth pressure distributions are desired in high-solidity applications.

Local Constriction Corrections

Corresponding to the velocity distributions, the local constriction corrections by conformal mapping (figs. 4 and 5) vary widely along the chord as well as fluctuate locally. The local constriction correction by the first-order image theory, although not giving any indication of fluctuations, agrees satisfactorily with the mapping correction up to solidities of about 1. Although the maximum corrections continue to agree fairly well at the higher solidities, the first-order image theory gives substantially higher corrections toward the extremities than the mapping theory.

The second-order image theory gives a better indication of the trend of the local constriction correction than the first-order image theory, although the indication is not much better for the 24-percent-thick airfoil. At solidities greater than 1, the second-order image theory substantially underestimates the correction toward the airfoil extremities and at the solidity of 2.0,overestimates the maximum value of the correction.

Average Constriction Corrections

The constriction corrections by the different theories were averaged in the range of 10 percent to 90 percent of the chord (this range was taken because of the difficulty at high solidity in obtaining sufficiently accurate cascade velocities by conformal mapping outside it) and are plotted against the parameter tc/h^2 in figure 6. The parameter tc/h^2 was chosen as the abscissa because first-order image theory gives (a) an almost linear variation of the average correction with this parameter (the variation is not exactly linear because the local constriction correction as derived in this paper depends on the exact isolated-airfoil velocity distribution, (see appendix D) and (b) a difference in slope for different airfoils, which largely depends on shape of the airfoil and not on over-all dimensions of the airfoil relative to the tunnel. (See appendix D.) Interpolation for average corrections for other airfoils is thereby facilitated. The average corrections by all methods are seen to bear an approximately linear relation to the parameter tc/h^2 and to differ substantially in slope among each other. A quantitative range of validity for the approximate methods is discussed in the next section.

For convenience in application, the average corrections are plotted in figure 7 as functions of tc/h^2, c/h, and t/h. It may be noted from figure 7(c) that for a given percentage of tunnel blocked area, that is, a given t/h, the average constriction correction is greater for a long airfoil than for a short one of the same shape, evidently because a longer airfoil experiences maximum constriction over a greater proportion of its length. The effect of shape is shown by the Kaplan section, which, for a given thickness ratio, has much greater peak velocities than sections of the low-drag type.

Range of Validity

The range of validity of the constriction corrections obtained by the different methods depends on the criterion used. If profile drag of the airfoil is considered, in order that the profile drag is not to be in error by more than 1 percent as a result of an error in the average constriction correction, the difference in average constriction corrections by the various methods should be less than approximately one-half of 1 percent, or

$$\left(\frac{\Delta v}{V}\right)_{av\ mapping} - \left(\frac{\Delta v}{V}\right)_{av\ image} < 0.005$$

It is shown in figure 6 that the range of validity for the first-order image correction is approximately $tc/h^2 < 0.08$ for both airfoils and for the second-order image correction, $tc/h^2 < 0.32$ for the 12-percent-thick airfoil and $tc/h^2 < 0.08$ for the 24-percent-thick airfoil.

A criterion for the validity of the constriction correction can also be taken as the accuracy of estimation of the critical compressibility speed of the isolated airfoil from measurement of the tunnel velocity distribution. Thus, the exact maximum velocity of the isolated airfoil was used to find the critical Mach number of the isolated airfoil, by Kármán's equation (65) of figure 13 (reference 6). The critical Mach numbers corresponding to the first- and second-order image theories were determined by using the maximum velocity of the distribution obtained by subtracting the respective local image correction from the local conformal-mapping tunnel-velocity distributions. The various critical Mach numbers thus found are given for the different cases in table IX. The table indicates that the approximate range of validity of the first-order image theory for estimation of critical speeds is $tc/h^2 < 0.12$ and 0.06 for the 12- and 24-percent-thick airfoils. The corresponding limit in the second-order image theory is approximately $tc/h^2 < 0.24$ for the 12- and 24-percent-thick airfoils.

CONCLUSIONS

The calculations and the conclusions of this paper relate to the comparison of the defined constriction corrections as calculated by different methods. The important question as to whether the constriction correction has physical meaning or validity in extreme cases is not considered herein. Hence, on the basis of the analysis and calculations of this paper, made on the assumptions of non-viscous, incompressible, two-dimensional flow, the following conclusions are indicated:

1. The difference between the velocity distribution of an airfoil in a tunnel and of the airfoil in a free stream, called the local constriction correction, varies widely over the chord for values of blocked-off tunnel area $t/h > 0.12$ where t is the maximum thickness of the airfoil and h is the height of the tunnel.

2. The local constriction corrections obtained by the Goldstein second-order image theory agree with those calculated by conformal mapping better than those calculated by first-order image theory. Both image theories substantially depart from the exact results of the conformal-mapping theory for $t/h > 0.12$.

3. The average constriction correction obtained by all methods increases approximately linearly with the parameter tc/h^2 where c is the chord of the airfoil.

4. Based on the criterion that isolated-airfoil profile drag determined from tunnel investigations shall not be in error by more than 1 percent because of constriction correction, the range of validity of the first-order theory is approximately $tc/h^2 < 0.08$ for 12-percent- and 24-percent-thick airfoils, and of the Goldstein second-order theory, $tc/h^2 < 0.32$ for 12-percent-thick airfoils and $tc/h^2 < 0.08$ for 24-percent-thick airfoils.

5. Based on the criterion that the critical compressibility speed of an isolated airfoil determined by tunnel velocity-distribution measurement shall not be in error by more than 1 percent because of constriction correction, the range of validity of the first-order image theory is approximately $tc/h^2 < 0.12$ and of the Goldstein second-order theory, approximately $tc/h^2 < 0.24$.

6. Curvature irregularities in the surface of an airfoil that are insufficient to cause observable irregularities in the isolated-airfoil velocity distribution can cause appreciable irregularities at $c/h > 1$. The first- and second-order image theories do not yield such irregularities.

7. The stream-filament theory, with simple account taken of the curvature of the streamlines, yields velocity distributions that agree well with those by conformal mapping for $c/h > 1$.

Flight Propulsion Research Laboratory,
National Advisory Committee for Aeronautics,
Cleveland, Ohio, March 18, 1948.

APPENDIX A

CONFORMAL MAPPING: METHOD OF FINITE CHORD

488

The flow through an unstaggered cascade of airfoils is determined in this method by the conformal transformation relating the cascade of airfoils, z-plane; the cascade of extended chord lines of the airfoils, ζ-plane; and the unit circle, p-plane.

The function by which the mapping is accomplished, the so-called Cartesian mapping function, is taken as the vector distance between conformally corresponding points in the z- and ζ-planes,

$$z - \zeta = \Delta x + i\Delta y \tag{A1}$$

This function is regular everywhere outside the circle in the p-plane and, hence, expressible by the inverse power series

$$z - \zeta = \sum_{0}^{\infty} \frac{c_n}{p^n} \qquad (c_n = a_n + ib_n) \tag{A2}$$

The relation between ζ and p is the known transformation from an unstaggered cascade of straight lines to a unit circle

$$\zeta = \tau + \log_e \frac{(e^K+p)(p+e^{-K})}{(e^K-p)(p-e^{-K})} \tag{A3}$$

where τ and K are real constants that determine the positions and the solidity of the cascade, respectively. (See references 1 and 2 for details regarding the formulas of this section.)

On the unit circle

$$p = e^{i\varphi}$$

$$x = \tau + \log_e \frac{\cosh K + \cos \varphi}{\cosh K - \cos \varphi} + \Delta x(\varphi) \tag{A4}$$

and

$$y = \Delta y(\varphi) \tag{A5}$$

where x and y are the abscissas and ordinates of the airfoil and φ is the central angle of the unit circle. The functions $\Delta x(\varphi)$ and $\Delta y(\varphi)$ are related either by the conjugate Fourier series, directly derivable from equation (A2) upon substitution of $p = e^{i\varphi}$, or by the integral relations:

$$\Delta x(\varphi) = -\frac{1}{2\pi}\int_0^{2\pi} \Delta y(\varphi') \cot\frac{\varphi'-\varphi}{2}\, d\varphi' \tag{A6}$$

488

$$\Delta y(\varphi) = \frac{1}{2\pi}\int_0^{2\pi} \Delta x(\varphi') \cot\frac{\varphi'-\varphi}{2}\, d\varphi' \tag{A7}$$

Given the airfoil coordinates x and y, equations (A4), (A5), and (A6) can be solved for the mapping function $\Delta x(\varphi) + i\Delta y(\varphi)$ by the following method of successive approximation: The upper surface of the airfoil is drawn with its leading- and trailing-edge chordwise extremities at the points $(\pi\sigma, 0)$, $(-\pi\sigma, 0)$, respectively, where σ is the solidity c/h. This form of the airfoil is referred to as the normal form. For a conveniently chosen set of values of the variable φ from 0° to 180° the airfoil ordinates $\Delta y(\varphi)$ are measured at the chordwise stations x (equation (A4)) corresponding to some appropriate initial abscissa function $\Delta x(\varphi)$, such as that of the previous approximation, or $\Delta x(\varphi) \equiv 0$, if there is no previous approximation. The function $\Delta x(\varphi)$ is computed from this $\Delta y(\varphi)$ by equation (A6). (See appendix C.) The constants K and τ are next determined from the $\Delta x(\varphi)$ function by means of the equations

$$\sinh K = \frac{1}{\sinh\left[\frac{\pi\sigma}{2}\,\frac{\Delta x(\pi) - \Delta x(0)}{4}\right]} \tag{A8}$$

$$\tau = -\frac{1}{2}\left[\Delta x(0) + \Delta x(\pi)\right] \tag{A9}$$

The constants K and τ so determined, together with the corresponding mapping function $\Delta x(\varphi) + i\Delta y(\varphi)$, yield a derived airfoil contour by equations (A4) and (A5), which is in the normal form and can be compared with the given airfoil. If the agreement is not sufficiently close, the foregoing procedure is repeated.

After the mapping function relating the circle and airfoil planes has been found, the velocity in the airfoil planes can be determined from the general equation

$$v_c = V\left|\frac{d\zeta}{dz}\right| \tag{A10}$$

488 The resulting formula for the velocity distribution on the airfoil itself is

$$\frac{v_c}{V} = \frac{2 \cosh K \; |\sin\varphi|}{(\sin^2\varphi + \sinh^2 K)\sqrt{\left(\left[\frac{d\zeta}{dp}\right] - \frac{d\Delta x}{d\varphi}\right)^2 + \left(\frac{d\Delta y}{d\varphi}\right)^2}} \tag{A11}$$

where

$$\left[\frac{d\zeta}{dp}\right] = \frac{2 \cosh K \sin\varphi}{\sin^2\varphi + \sinh^2 K} \tag{A12}$$

The details of the calculation of the conjugate derivatives $d\Delta x/d\varphi$ and $d\Delta y/d\varphi$ from the known functions $\Delta x(\varphi)$ and $\Delta y(\varphi)$ are given in appendix C.

For the limiting case of the isolated airfoil, three of the six calculating equations (A4), (A5), (A6), (A8), (A9), and (A11) must be changed, namely, (A4), (A8), and (A11). The corresponding equations are, respectively,

$$x = \tau + r \cos\varphi + \Delta x(\varphi) \tag{A4'}$$

$$r = 1 + \frac{\Delta x(\pi) - \Delta x(0)}{2} \tag{A8'}$$

$$\frac{v_i}{V} = \frac{|\sin\varphi|}{\sqrt{\left(\sin\varphi - \frac{d\Delta x}{r d\varphi}\right)^2 + \left(\frac{d\Delta y}{r d\varphi}\right)^2}} \tag{A11'}$$

The quantity r is the diameter of the circle to which the isolated airfoil is conformally related.

The calculations by the method of finite chord were for the most part based on the set of 12 evenly spaced φ values, 0°, 15°, . . ., 180°. The leading edge of the airfoil corresponded to

$\varphi = 0^{\circ}$ and the trailing edge to 180°. The symmetry of the airfoil and its position has a corresponding symmetry in the mapping function and its derivatives; namely,

$$\left.\begin{array}{l} \Delta x(\varphi) \\ \Delta y(\varphi) \\ d\Delta x/d\varphi \\ d\Delta y/d\varphi \end{array}\right\} \text{is an} \left\{\begin{array}{l} \text{even} \\ \text{odd} \\ \text{odd} \\ \text{even} \end{array}\right\} \begin{array}{l} \text{function with respect to} \\ \text{the station } \varphi = \pi. \end{array}$$

APPENDIX B

CONFORMAL MAPPING: METHOD OF SEMI-INFINITE CHORD

In this method the flow through the unstaggered cascade of airfoils is determined by the conformal transformation relating the cascade of shapes consisting of the airfoils and their zero streamline prolongation in one direction, z-plane, the cascade of semi-infinite straight chord lines, ζ-plane, and the unit circle, p-plane.

The essential difference between this method and the method of finite chord lies in the relation between the ζ- and p-planes. In this case the relation is

$$\zeta = \frac{h}{2\pi} \log_e \left[1 - \left(\frac{p+1}{p-1}\right)^2\right] - 1 \tag{B1}$$

This function transforms the unit circle in the p-plane into an unstaggered cascade of semi-infinite straight lines of which the abscissas range from -1 to $+\infty$. The term $(p+1)/(p-1)$ transforms the unit circle into an infinite straight line; squaring the term yields a semi-infinite straight line; and the logarithm transforms the straight line into a cascade of straight lines. The vertical distance between two consecutive lines is h. On the unit circle

$$p = e^{i\varphi}$$

$$x = \frac{-2}{\pi\sigma} \log\left|\sin \frac{\varphi}{2}\right| - 1 + \Delta x(\varphi) - \Delta x(180^\circ) \tag{B2}$$

$$y = \Delta y(\varphi) \tag{B3}$$

where all lengths are expressed as fractions of airfoil chord c, which was taken as $c = 2$, and the term $\Delta x(180^\circ)$ has been inserted in order to locate the airfoils of the successive approximations with one extremity at the point $(-1, 0)$.

The velocity distribution on the airfoil given by equation (A10) now becomes

$$\frac{v_c}{V} = \frac{\frac{1}{\pi\sigma} \cot \frac{\varphi}{2}}{\sqrt{\left(\frac{1}{\pi\sigma} \cot \frac{\varphi}{2} - \frac{d\Delta x}{d\varphi}\right)^2 + \left(\frac{d\Delta y}{d\varphi}\right)^2}} \tag{B4}$$

No intermediate adjustment such as is represented by equation (A8) is required; hence the solution by successive approximation outlined in appendix A is reduced to little more than the calculation of conjugates.

The chordwise stations for an evenly spaced set of φ-points tend to cluster around $x = -1$ with the transformation (B2). Consequently, in order to obtain a sufficiently even distribution of points over the airfoil, two devices were resorted to. The first was to perform the calculation twice for each case. The airfoil was first considered with the leading edge at $x = -1$ and the trailing edge at $x = 1$ and a solution obtained for the mapping function. The airfoil was then considered as reversed with respect to the y-axis and a solution obtained for another mapping function. The set of φ-points was the same in both solutions. The second device, which is applicable more generally in conformal-mapping problems, consisted in using a standard set of θ-points in a p'-plane related to the p-plane by the bilinear transformation

$$p = \frac{p' + \frac{n-1}{n+1}}{\frac{n-1}{n+1}p' + 1} \tag{B5}$$

The transformation (B5) is so chosen that (a) the unit circle $p = e^{i\varphi}$ goes into the unit circle $p' = e^{i\theta}$ with the points $p = \pm 1$ corresponding to $p' = \pm 1$ and the outside spaces corresponding, and (b) the derivative $\left(\frac{dp'}{dp}\right)_{p=1} = n$. By condition (a), the conjugate relation (A6) is valid in the p'-plane. Condition (b) causes a small range ϵ $(\epsilon = \varphi - \theta)$ of φ near $\varphi = 0$, which corresponds to $x = \infty$, to correspond, for $n > 1$, to a larger range $n\epsilon$ of θ near $\theta = 0$. Hence, for $n > 1$, an evenly spaced set of θ-points yields a more evenly distributed set of chordwise stations x than the same spacing of φ-points. The values of φ corresponding to the assumed θ-points are obtained from equation (B5) with $p = e^{i\varphi}$, $p' = e^{i\theta}$,

$$\tan \varphi = \frac{2n \sin \theta}{(n^2-1) + (n^2+1) \cos \theta} \tag{B6}$$

The conjugate derivatives in the velocity formula (B4) were obtained by

$$\left.\begin{aligned} \frac{d\Delta x}{d\varphi} &= \frac{d\Delta x}{d\theta}\frac{d\theta}{d\varphi} \\ \frac{d\Delta y}{d\varphi} &= \frac{d\Delta y}{d\theta}\frac{d\theta}{d\varphi} \end{aligned}\right\} \tag{B7}$$

with

$$\frac{d\theta}{d\varphi} = \frac{(n^2-1)\cos\theta + (n^2+1)}{2n} \tag{B8}$$

The derivatives $d\Delta x/d\theta$ and $d\Delta y/d\theta$, in the cases treated by the method of semi-infinite chord ($\sigma = 1.0, 1.5, 2.0$), were measured graphically by drawing tangents to the calculated curves $\Delta x(\theta)$ and $\Delta y(\theta)$. This procedure was found to be more accurate at high solidities than that of calculating the derivatives by the formulas given in appendix C.

A typical result obtained by the method of semi-infinite chord is illustrated in figure 8. The quantity n was so chosen that the points obtained for the front half of the airfoil overlapped the points obtained for the rear half of the airfoil. The resulting values of n ranged from 2 to 30 and are given for each case in tables II and III. The calculations were based in the case $\sigma = 1$ on the use of 12 evenly spaced values of $\theta = 0^\circ, 15^\circ, \ldots, 180^\circ$ and for the higher solidities on the 24 values $\theta = 0^\circ, 7.5^\circ, 15^\circ, \ldots, 180^\circ$.

It may be noted that the effect of boundary-layer development along and downstream of the airfoil can be taken into account quite simply in this method by considering as boundary contour the locus of the outer edge of the displacement boundary layer along and downstream of the airfoil.

The effect of boundary-layer development on the tunnel walls can be treated by so altering the mapping problem that the channel between the zero streamline of the airfoil and one tunnel wall is to be mapped into a uniform channel. The mapping methods for this problem are similar to those already described.

APPENDIX C

NUMERICAL EVALUATION OF CONJUGATE FUNCTIONS

AND THEIR DERIVATIVES

The determination of the conjugate function $\Delta x(\varphi)$ and of the conjugate derivatives $d\Delta x/d\varphi$, $d\Delta y/d\varphi$ from a known function $\Delta y(\varphi)$ was based in this paper on numerical integration of equation (A6) and, for solidities of 0 and 0.5, integration of the respective derivatives of equations (A6) and (A7). After several trials with other methods of evaluation, including Fourier expansion, graphical methods, and various kinds of numerical integration, the following procedures were adopted as a compromise between accuracy and expenditure of effort.

In order to calculate $\Delta x(\varphi)$, the range of integration in equation (A6) was divided into an even number of equal intervals. The function $\Delta y(\varphi)$ was considered to be known numerically at the values of φ separating these intervals. In the region outside the intervals on either side of the singular point $\varphi = \varphi'$, the integral was evaluated by Simpson's rule. The contribution to the integral of the two intervals separated by the singular point φ' was obtained by representing $\Delta y(\varphi)$ in this range by the form

$$\Delta y(\varphi) = A \cos \varphi + B \sin \varphi + C \tag{C1}$$

The constants A, B, and C were so determined that equation (C1) was satisfied at the three φ-points bounding the two intervals. The final result for $\Delta x(\varphi)$ is an expression of the form

$$\Delta x(\varphi) = \sum_{k=0}^{2n-1} a_k \, \Delta y(\varphi + k\delta) \tag{C2}$$

where δ is the interval between two consecutive values of φ and $2n\delta = 2\pi$. The 24 coefficients a_k for $n = 12$ are listed in table VII.

The conjugate derivatives $d\Delta x/d\varphi$ and $d\Delta y/d\varphi$ were obtained in an analogous manner from the relations

$$\frac{d\Delta x(\varphi)}{d\varphi} = -\frac{1}{4\pi}\int_0^{2\pi} \frac{\Delta y(\varphi') - \Delta y(\varphi)}{\sin^2 \frac{\varphi' - \varphi}{2}} \, d\varphi' \tag{C3}$$

488

$$\frac{d\Delta y(\varphi)}{d\varphi} = \frac{1}{4\pi}\int_0^{2\pi} \frac{\Delta x(\varphi') - \Delta x(\varphi)}{\sin^2 \frac{\varphi' - \varphi}{2}}\, d\varphi' \tag{C4}$$

These relations can be derived by differentiating equations (A6) and (A7) under the integral sign after subtracting $\Delta y(\varphi)$ and $\Delta x(\varphi)$ from the respective integrands to make this operation permissible. They can also be obtained by a limiting process in the complex plane similar to that of reference 1, appendix C. The numerical integration of equations (C3) and (C4) by Simpson's rule and a sinusoidal approximation over the singularity result as before in expressions of the form

$$\frac{d\Delta x}{d\varphi} = -\sum_{k=0}^{2n-1} b_k\, \Delta y(\varphi + k\delta) \tag{C5}$$

$$\frac{d\Delta y}{d\varphi} = \sum_{k=0}^{2n-1} b_k\, \Delta x(\varphi + k\delta) \tag{C6}$$

The b_k coefficients are listed in table VII for $n = 12$. The a_k and b_k coefficients were also calculated for 48 φ-points, and are listed in table VIII.

Explicit expressions for the coefficients for a $2n$-point scheme are $(2n\,\delta = 2\pi)$

$$\left.\begin{aligned}
a_0 &= 0\\
a_1 &= -\frac{\delta}{6\pi}\cot\frac{\delta}{2} - \frac{\delta + \sin\delta}{2\pi\sin\delta}\\
a_{2n-1} &= \frac{\delta}{6\pi}\cot\frac{\delta}{2} + \frac{\delta + \sin\delta}{2\pi\sin\delta}\\
a_k &= -\frac{\delta}{3\pi}\cot\frac{k\delta}{2} \qquad (k \text{ odd})\\
a_k &= -\frac{2\delta}{3\pi}\cot\frac{k\delta}{2} \qquad (k \text{ even})
\end{aligned}\right\} \tag{C7}$$

$$\left.\begin{aligned}
b_0 &= -\sum_{k=2}^{2n-2} b_k - \frac{\delta}{6\pi \sin^2 \frac{\delta}{2}} - \frac{\delta}{\pi(1 - \cos \delta)} \\
b_1 = b_{2n-1} &= \frac{\delta}{12\pi \sin^2 \frac{\delta}{2}} + \frac{\delta}{2\pi (1 - \cos \delta)} \\
b_k &= \frac{\delta}{3\pi \sin^2 \frac{k\delta}{2}} \qquad (k \text{ even}) \\
b_k &= \frac{\delta}{6\pi \sin^2 \frac{k\delta}{2}} \qquad (k \text{ odd})
\end{aligned}\right\} \qquad \text{(C8)}$$

488

The accuracy of the 24- and 48-point schemes was checked on the function $\sin 2\varphi$. The 24-point scheme gave results for the conjugate accurate to 0.8 percent and for the derivatives accurate to 0.2 percent. The 48-point scheme resulted in 0.2-percent accuracy for the conjugate and 0.05-percent accuracy for the derivatives. These values for accuracy are given only as a reference with which to compare other methods. They do not give any direct indication of the accuracy of evaluation of the conjugate functions and derivatives of this paper.

APPENDIX D

FIRST-ORDER IMAGE THEORY

In this method of obtaining the constriction correction, the image airfoils (fig. 1) are replaced by equivalent doublets. The disturbance velocity produced in the region of the physical airfoil by these doublets is u and the resultant velocity is therefore $V + u$. The tunnel velocity distribution of the airfoil v_c is assumed to be given by its nondimensional isolated-airfoil velocity distribution v_i/V multiplied by the velocity $V + u$; that is,

$$\frac{v_c}{V + u} = \frac{v_i}{V} \tag{D1}$$

so that the constriction correction is

$$\frac{\Delta v}{V} = \frac{v_c - v_i}{V} = \frac{v_i}{V}\frac{u}{V} \tag{D2}$$

According to Glauert (reference 3, p. 53), the disturbance velocity u is given by

$$\frac{u}{V} = \frac{\pi^2}{12}\lambda\left(\frac{t}{h}\right)^2 \tag{D3}$$

where the factor λ is given by

$$\lambda = \frac{4}{\pi}\frac{c}{t}\int\frac{v_c}{V}\frac{y}{t}\,d\left(\frac{s}{c}\right) \tag{D4}$$

(reference 3, p. 55; Glauert does not explicitly indicate the chord c and his q is here v_c in accordance with his explanation of the evaluation of λ). The integral in equation (D4) is taken with respect to surface distance s along the upper surface of the airfoil from leading to trailing edge. Its form indicates that λ is approximately inversely proportional to t/c (see also reference 3, equation (17.10)), and thus u/V is proportional to the parameter tc/h^2. The values of λ calculated from equation (D4) for the various cases are given in table X.

The constriction correction given by equation (D2) represents a refinement of the usually given first-order constriction correction u/V, which is a constant along the chord. This procedure is used in order to be consistent with the constriction correction derived from Goldstein's theory as discussed in appendix E.

It may be noted that in calculating the strength of a doublet that is to replace an isolated airfoil, v_i rather than v_c should be used in equation (D4). However, inasmuch as the strength of the doublet must be increased when it is used to replace the same airfoil in a cascade, the use of v_c, which is greater than v_i, will 488
change the value of λ in the right direction. For the low values of the solidity for which the doublet correction is used, however, there is no appreciable difference in the correction.

APPENDIX E

SECOND-ORDER IMAGE THEORY

Goldstein (reference 4) first replaces the image airfoils (fig. 1) by the doublet and higher-order singularities given by the potential function of the airfoil in a uniform free stream. The nonuniform disturbance velocity produced by these singularities in the physical region, in particular at the location of the physical airfoil, is calculated. This first-approximation nonuniform disturbance velocity (a) changes the velocity distribution of the airfoil from its isolated free-stream value and (b) changes the values of the singularities that are to be imaged. Change (b) is evaluated and a second-approximation nonuniform disturbance velocity is calculated, etc., to higher approximations. Lastly, the velocity distribution of the airfoil in the final nonuniform stream is calculated.

In principle, Goldstein's method is capable of yielding to any degree of accuracy the effect of a tunnel on the two-dimensional velocity distribution of an arbitrary airfoil, arbitrarily situated. The successive approximations, however, become increasingly laborious. Goldstein gives the formulas to the second approximation; that is, to the order tc^3/h^4, t^2c^2/h^4, t^3c/h^4. These formulas are quoted here as used in, and in the notation of, this paper.

The fundamental formula for the symmetrical constriction correction is obtained as the ratio of tunnel to free-stream velocity distribution:

$$\frac{v_c}{v_i} = \frac{U}{V}\left(1 + \frac{P(\theta)}{\sin\,\theta}\right) \tag{E1}$$

so that

$$\frac{\Delta v}{V} = \frac{v_c - v_i}{V} = \frac{v_i}{V}\left(\frac{v_c}{v_i} - 1\right) \tag{E2}$$

where

$$\frac{U}{V} = 1 + \frac{4}{3}\,S^2 d_1 + \frac{2}{9}\,S^4\left(8d_1{}^2 - \frac{24}{5}\,d_3\right) \tag{E3}$$

$$\begin{aligned} P(\theta) = {} & \lambda_2{}'\,(R\,\sin\,2\theta - A_0 \sin\,\theta) \\ & + \lambda_3{}'\,(R^2 \sin\,3\theta - 2RA_0 \sin\,2\theta + A_0{}^2 \sin\,\theta - A_1 \sin\,\theta) \end{aligned} \tag{E4}$$

$$S = \frac{\pi}{2h} \tag{E5}$$

$$\left.\begin{aligned} \lambda_2' &= \frac{2\pi^4}{15c^4}\left(\frac{c}{h}\right)^4 d_2 \\ \lambda_3' &= -\frac{\pi^4}{15c^4}\left(\frac{c}{h}\right)^4 d_1 \end{aligned}\right\} \tag{E6}$$

$$\left.\begin{aligned} R &= \frac{c}{4}(1 + C_0) \\ A_n &= B_n \\ B_0 &= -\frac{c}{4} C_1 \\ B_1 &= -\frac{c^2}{16}(1 + C_2) \\ B_2 &= -\frac{c^3}{64} C_3 \end{aligned}\right\} \tag{E7}$$

$$\left.\begin{aligned} d_1 &= \frac{c^2}{16}(2C_0 - C_2) \\ d_3 &= -\frac{c^4}{256} C_4 \end{aligned}\right\} \tag{E8}$$

$$\left.\begin{aligned} C_0 &= \frac{2}{\pi c}\int_0^\pi \frac{y(\theta)}{\sin\theta}\,d\theta \\ C_n &= \frac{4}{\pi c}\int_0^\pi \frac{y(\theta)\cos n\theta}{\sin\theta}\,d\theta, \; n > 0 \end{aligned}\right\} \tag{E9}$$

where $y(\theta)$ is the airfoil ordinate corresponding to the abscissa and $\theta = 0$ corresponds to the leading edge of the airfoil.

$$x = \frac{c}{2}\cos\theta \tag{E10}$$

Equation (E1) corresponds to Goldstein's equation (97) (p. 48) of reference 4. The factor U/V has been inserted to reduce the isolated-airfoil velocity, Goldstein's q_1, from U to V as the free-stream velocity. Equations (E3) to (E6) correspond respectively to Goldstein's equations (40) (p. 37), (99) (p. 48), (21) (p. 34), and (100) (p. 48). Equations (E7) to (E10) correspond to those of appendix 5 (p. 21).

The basic constants C_n calculated in this paper are given in table X on the basis that the airfoil chord be 2.

The velocity distribution by conformal mapping was used for v_i/V in equations (E2) and (D2) because it had already been calculated. It would have been somewhat more consistent to use the velocity distributions derived by thin-airfoil theory inasmuch as the constants C_n (equation (E9)) were so derived. The differences between the two distributions, being of the orders $(t/c)^2$, $(t/c)^3$, . . ., do not affect the main contribution to the second order of Goldstein's results, namely, the contribution of the order tc^3/h^4.

It is noted that in applying equation (E3) to thin airfoils, Goldstein in his equation (75) (p. 45) neglects the term d_1^2. This term was not found to be negligible in the calculations of this paper and was retained.

APPENDIX F

STREAM-FILAMENT THEORY

The irrotational motion of an ideal incompressible fluid is completely determined by the equations of irrotationality and continuity of mass and by the boundary conditions. Consider the equation of irrotationality in the form (reference 6, equation (41))

$$\frac{\partial v}{\partial n} + \frac{v}{R} = 0 \qquad \text{(F1)}$$

where

n distance along potential line at point of flow field

R radius of curvature of streamline at same point of flow field; positive if streamline is convex in positive n direction.

Introduce the approximations (a) that the potential lines are straight lines perpendicular to the x-axis, or

$$n = y \qquad \text{(F2)}$$

and (b) that the curvature of the streamlines at any chordwise location varies linearly from its known value at the airfoil to the known value, 0, at the wall, or

$$1/R = C = C_a \frac{(h/2) - y}{(h/2) - Y} \qquad Y < y < h/2 \qquad \text{(F3)}$$

where

C curvature of streamline at chordwise station X

C_a curvature of airfoil surface at chordwise station X

Y ordinate of airfoil at chordwise station X

The boundary condition that the boundaries be streamlines is satisfied by equation (F3). Substitution of equations (F2) and (F3) into (F1) and integration yields

$$v = F(x)e^{\frac{C_a}{2} \frac{(h/2-y)^2}{(h/2-Y)}}$$

where $F(x)$ is an arbitrary function fixed by the condition of continuity. Integrating equation (F4) with respect to y from Y to $h/2$ gives the flow quantity $(h/2)V$ to the approximation underlying equations (2) and (3); that is,

488

$$V \frac{h}{2} = \int_{Y}^{h/2} v dy = F(x) \int_{Y}^{h/2} e^{\frac{C_a}{2} \frac{(h/2-y)^2}{(h/2-Y)}} dy \tag{F5}$$

When this equation is solved for $F(x)$ and substituted in equation (F4), there results for the velocity at any point of the flow field

$$\frac{v}{V} = \frac{h/2 \; e^{\frac{C_a}{2} \frac{(h/2-y)^2}{(h/2-Y)}}}{\int_{Y}^{h/2} e^{\frac{C_a}{2} \frac{(h/2-y)^2}{(h/2-Y)}} dy} \tag{F6}$$

Expressing all lengths, including the radius of curvature, as fractions of airfoil chord c and making the substitutions

$$t = \sqrt{\frac{C_a}{4\sigma} \frac{(1-2\sigma y)^2}{1-2\sigma Y}} \tag{F7}$$

and

$$T = \sqrt{\frac{C_a}{4\sigma} (1-2\sigma Y)} \tag{F8}$$

where

$$\sigma = c/h$$

and

$$C_a = C_a(X) = \frac{d^2Y/dX^2}{\left[1 + \left(\frac{dY}{dX}\right)^2\right]^{3/2}} \tag{F9}$$

equation (F6) becomes 488

$$\frac{v}{V} = \frac{Te^{T^2\left(\frac{1-2\sigma y}{1-2\sigma Y}\right)^2}}{(1 - 2\ Y)\int_0^T e^{t^2}dt} \tag{F10}$$

At the airfoil, equation (F10) gives finally

$$\left(\frac{v}{V}\right)_a = \frac{Te^{T^2}}{(1 - 2\sigma Y)\int_0^T e^{t^2}dt} \tag{F11}$$

If $C_a = 0$, equation (F6) reduces to the simplest form of stream-filament theory, namely

$$\frac{v}{V} = \frac{h/2}{h/2 - Y} \tag{F12}$$

Equations (F8), (F9), and (F11) were used for the calculation of the velocity distributions of the airfoil in the tunnel by the stream-filament theory. The integral in equation (F11) is tabulated in reference 7 (p. 32).

This method may be useful in determining the influence of compressibility. For an ideal compressible fluid, the only change required in equation (F10) or (F11) is the insertion of the factor ρ/ρ_o under the integral sign, where ρ is the density of the fluid and ρ_o is the ultimate upstream density.

488

REFERENCES

1. Mutterperl, William: The Conformal Transformation of an Airfoil into a Straight Line and Its Application to the Inverse Problem of Airfoil Theory. NACA ARR No. L4K22a, 1944.

2. Mutterperl, William: A Solution of the Direct and Inverse Potential Problems for Arbitrary Cascades of Airfoils. NACA ARR No. L4K22b, 1944.

3. Glauert, H.: Wind Tunnel Interference on Wings, Bodies, and Airscrews. R. & M. No. 1566, A.R.C., 1933.

4. Goldstein, S.: Steady Two-Dimensional Flow past a Solid Cylinder in a Non-Uniform Stream and Two-Dimensional Wind-Tunnel Interference. R. & M. No. 1902, M.A.P., 1942.

5. Kaplan, Carl: The Flow of a Compressible Fluid Past a Curved Surface. NACA ARR No. 3K02, 1943.

6. von Kármán, Th.: Compressibility Effects in Aerodynamics. Jour. Aero. Sci., vol. 8, no. 9, July 1941, pp. 337-356.

7. Jahnke, Eugene, and Emde, Fritz: Tables of Functions with Formulae and Curves. Dover Publications (New York), 1943.

TABLE I. - ORDINATES OF AIRFOILS

Station (percent chord from nose)	Ordinate of 12-percent-thick airfoil	Ordinate of 24-percent-thick airfoil	Station (percent chord from nose)	Ordinate of 12-percent-thick airfoil	Ordinate of 24-percent-thick airfoil
0	0	0	50	5.880	11.810
1.25	1.425	2.250	55	5.540	11.380
2.5	1.900	3.285	60	5.025	10.665
5	2.585	4.620	65	4.415	9.735
10	3.540	6.455	70	3.750	8.575
15	4.250	7.890	75	3.060	7.250
20	4.820	9.050	80	2.350	5.825
25	5.295	10.070	85	1.685	4.365
30	5.655	10.885	90	1.060	2.925
35	5.900	11.495	95	.510	1.605
40	6.000	11.855	97.5	.260	.950
45	6.010	11.980	100	0	0

488

NACA

TABLE II. - VELOCITY DISTRIBUTIONS AND CARTESIAN MAPPING

FUNCTIONS FOR 12-PERCENT-THICK AIRFOIL

(a) c/h, 0; method of finite chord; r, 1.0896; τ, 0.0243

φ (deg)	Percent chord	$\frac{v_i}{V}$	x	Δy	Δx	$\frac{d\Delta x}{d\varphi}$	$\frac{d\Delta y}{d\varphi}$
0 × 15	0	0	1.0000	0	-0.1139	0	0.1200
1	1.625	1.0436	.9675	.0312	-.1093	.0363	.1121
2	6.480	1.0834	.8704	.0578	-.0976	.0521	.1005
3	14.24	1.1136	.7151	.0837	-.0797	.0845	.0908
4	24.24	1.1303	.5151	.1045	-.0540	.1117	.0695
5	35.70	1.1574	.2861	.1186	-.0202	.1436	.0305
6	47.80	1.1690	.0441	.1195	.1098	.1582	-.0347
7	60.06	1.1191	-.2012	.1008	.0565	.1183	-.0999
8	72.11	1.0422	-.4422	.0693	.0783	.0465	-.1233
9	83.15	.9821	-.6630	.0389	.0832	-.0072	-.1032
10	92.08	.9400	-.8416	.0168	.0777	-.0309	-.0660
11	97.94	.8996	-.9588	.0042	.0694	-.0301	-.0300
12	100.00	0	-1.0000	0	.0653	0	-.0127

(b) c/h, 0.5; method of finite chord; cosh k, 1.43094; τ, 0.04158

φ (deg)	Percent chord	$\frac{v_c}{V}$	$\frac{x}{0.5\pi}$	$\frac{\Delta y}{0.5\pi}$	Δx	$\frac{d\Delta x}{d\varphi}$	$\frac{d\Delta y}{d\varphi}$
0 × 15	0	0	1.0000	0	-0.2008	0	0.2331
1	2.515	1.0792	.9497	.0381	-.1897	.0850	.2081
2	9.190	1.1087	.8162	.0682	-.1623	.1218	.1644
3	18.20	1.1284	.6360	.0925	-.1256	.1558	.1269
4	28.02	1.1543	.4396	.1103	-.0806	.1872	.0830
5	37.96	1.1714	.2409	.1195	-.0290	.2046	.0291
6	47.82	1.1843	.0436	.1195	.0269	.2182	-.0411
7	57.76	1.1485	-.1552	.1059	.0805	.1865	-.1205
8	68.08	1.0789	-.3616	.0805	.1200	.1123	-.1713
9	78.74	1.0150	-.5747	.0507	.1387	.0314	-.1762
10	88.94	.9614	-.7789	.0236	.1376	-.0362	-.1360
11	96.90	.9207	-.9379	.0062	.1250	-.0541	-.0675
12	100.00	0	-1.0000	0	.1177	0	-.0311

NACA

TABLE II. - VELOCITY DISTRIBUTIONS AND CARTESIAN MAPPING

FUNCTIONS FOR 12-PERCENT-THICK AIRFOIL - Continued

(c) c/h, 1.0; method of semi-infinite chord; c, 2; h, 2; n, 4

θ (deg)	Percent chord	$\frac{v_c}{V}$	x	φ (deg)	Δy	Δx	$\frac{d\Delta x}{d\varphi}$	$\frac{d\Delta y}{d\varphi}$
Front half of airfoil								
0 × 15	∞	1.0000	∞	0	0	-0.1088	0	0
1	95.70	.9607	0.9139	3.770	.0086	-.1214	-.3324	1.1276
2	73.04	1.0742	.4608	7.665	.0667	-.1232	.3682	.5940
3	60.81	1.1637	.2162	11.824	.0988	-.0924	.4510	.3130
4	52.16	1.2215	.0431	16.426	.1151	-.0573	.4040	.1207
5	44.92	1.2192	-.1015	21.718	.1203	-.0258	.2984	.0162
6	38.34	1.2117	-.2333	28.072	.1197	.0032	.2227	-.0212
7	31.88	1.2043	-.3625	36.092	.1153	.0299	.1668	-.0413
8	25.27	1.1842	-.4946	46.826	.1064	.0563	.1165	-.0519
9	18.16	1.1595	-.6367	62.226	.0924	.0814	.0756	-.0523
10	10.56	1.1398	-.7888	86.030	.0726	.1061	.0452	-.0446
11	3.390	1.1275	-.9322	124.456	.0434	.1283	.0251	-.0424
12	0	0	-1.0000	180.000	0	.1384	0	-.0473
Rear half of airfoil								
0 × 15	$-\infty$	1.0000	∞	0	0	-0.1442	0	0
1	2.350	[a].9668	0.9530	3.770	.0368	-.1442	0	2.5559
2	23.64	[a]1.1938	.5273	7.665	.1039	-.1186	.7898	.3835
3	34.90	[a]1.2359	.3020	11.824	.1180	-.0686	.5881	.0842
4	43.40	1.2265	.1321	16.426	.1204	-.0302	.4073	-.0075
5	50.64	1.2145	-.0129	21.718	.1169	.0009	.2950	-.0731
6	57.26	1.1872	-.1453	28.072	.1065	.0293	.2061	-.1062
7	63.94	1.1367	-.2787	36.092	.0909	.0517	.1254	-.1092
8	70.98	1.0845	-.4197	46.826	.0721	.0692	.0636	-.0926
9	78.80	1.0382	-.5759	62.226	.0503	.0802	.0240	-.0679
10	87.44	.9922	-.7488	86.030	.0277	.0842	0	-.0428
11	95.94	.9591	-.9187	124.456	.0084	.0799	-.0063	-.0175
12	100.00	0	-1.0000	180.000	0	.0765	0	0

[a]Rejected points.

NACA

TABLE II. - VELOCITY DISTRIBUTIONS AND CARTESIAN MAPPING

FUNCTIONS FOR 12-PERCENT-THICK AIRFOIL - Continued

(d) c/h, 1.5; method of semi-infinite chord; c, 2; h, 4/3; n, 8

θ (deg)	Per cent chord	$\frac{v_c}{V}$	x	φ (deg)	Δy	Δx	$\frac{d\Delta x}{d\varphi}$	$\frac{d\Delta y}{d\varphi}$
Front half of airfoil								
0 × 7½	∞	1.0000	∞	0	0	-0.1819	0	0
1	84.68	[a]1.0101	0.6936	.939	.0340	-.1785	.4875	3.4182
2	70.72	[a]1.1157	.4145	1.886	.0732	-.1623	1.4512	1.6175
3	63.24	[a]1.1943	.2647	2.849	.0929	-.1363	1.4400	.8547
4	58.09	1.2407	.1618	3.837	.1048	-.1130	1.2561	.5231
5	54.10	1.2699	.0820	4.859	.1123	-.0928	1.0758	.3162
6	50.82	1.2851	.0163	5.928	.1169	-.0744	.9134	.1643
7	47.93	1.2842	-.0414	7.055	.1191	-.0580	.7629	.0769
8	45.34	1.2747	-.0931	8.256	.1201	-.0432	.6339	.0332
9	42.93	1.2707	-.1414	9.549	.1203	-.0300	.5413	.0067
10	40.64	1.2717	-.1872	10.958	.1202	-.0175	.4726	-.0078
11	38.43	1.2731	-.2314	12.512	.1198	-.0055	.4155	-.0270
12	36.28	1.2736	-.2745	14.250	.1189	.0064	.3652	-.0360
13	34.12	1.2694	-.3175	16.224	.1175	.0181	.3169	-.0467
14	31.94	1.2640	-.3612	18.505	.1152	.0298	.2733	-.0502
15	29.68	1.2556	-.4064	21.192	.1129	.0415	.2326	-.0549
16	27.31	1.2443	-.4538	24.433	.1096	.0537	.1945	-.0573
17	24.75	1.2339	-.5050	28.447	.1053	.0660	.1611	-.0571
18	21.98	1.2245	-.5605	33.585	.1006	.0791	.1317	-.0566
19	18.87	1.2119	-.6226	40.431	.0939	.0930	.1038	-.0536
20	15.32	1.1960	-.6935	50.019	.0854	.1077	.0776	-.0481
21	11.25	1.1792	-.7750	64.292	.0748	.1238	.0544	-.0420
22	6.655	1.1658	-.8669	87.030	.0588	.1414	.0355	-.0376
23	2.175	1.1432	-.9565	124.660	.0359	.1586	.0202	-.0344
24	0	0	-1.0000	180.000	0	.1666	0	-.0404
Rear half of airfoil								
0 × 7½	-∞	1.0000	∞	0	0	-0.2335	0	0
1	12.90	[a]1.1409	0.7420	.939	.0793	-.2066	3.3265	2.3963
2	25.22	[a]1.2399	.4955	1.886	.1064	-.1571	2.5341	.8991
3	32.14	[a]1.2787	.3571	2.849	.1156	-.1204	1.8673	.3051
4	37.14	1.2787	.2573	3.837	.1192	-.0938	1.3824	.1196
5	41.07	1.2631	.1786	4.859	.1203	-.0723	1.0420	.0359
6	44.38	1.2774	.1124	5.928	.1204	-.0543	.8901	-.0246
7	47.25	1.2879	.0550	7.055	.1198	-.0379	.7706	-.0716
8	49.84	1.2868	.0033	8.256	.1179	-.0229	.6580	-.1092
9	52.24	1.2776	-.0447	9.549	.1150	-.0093	.5564	-.1320
10	54.53	1.2604	-.0906	10.958	.1115	.0030	.4629	-.1433
11	56.76	1.2421	-.1352	12.512	.1075	.0146	.3844	-.1482
12	58.97	1.2257	-.1794	14.250	.1029	.0253	.3205	-.1487
13	61.20	1.2078	-.2241	16.224	.0976	.0353	.2647	-.1451
14	63.51	1.1891	-.2702	18.505	.0920	.0446	.2158	-.1373
15	65.90	1.1682	-.3181	21.192	.0861	.0537	.1717	-.1278
16	68.46	1.1466	-.3691	24.433	.0790	.0623	.1331	-.1152
17	71.22	1.1247	-.4245	28.447	.0715	.0703	.0998	-.1016
18	74.28	1.1028	-.4856	33.585	.0632	.0780	.0716	-.0876
19	77.72	1.0816	-.5545	40.431	.0534	.0850	.0485	-.0731
20	81.72	1.0504	-.6343	50.019	.0425	.0908	.0257	-.0579
21	86.40	1.0153	-.7279	64.292	.0300	.0948	.0076	-.0412
22	91.83	.9822	-.8366	87.030	.0170	.0956	-.0026	-.0256
23	97.31	.9559	-.9462	124.660	.0055	.0928	-.0046	-.0114
24	100.00	0	-1.0000	180.000	0	.0905	0	0

[a]Rejected points.

TABLE II. - VELOCITY DISTRIBUTIONS AND CARTESIAN MAPPING

FUNCTIONS FOR 12-PERCENT-THICK AIRFOIL - Concluded

(e) c/h, 2.0; method of semi-infinite chord; c, 2; h, 1; n, 15

θ (deg)	Percent chord	$\frac{v_c}{V}$	x	φ (deg)	Δy	Δx	$\frac{d\Delta x}{d\varphi}$	$\frac{d\Delta y}{d\varphi}$
	Front half of airfoil							
$0 \times 7\frac{1}{2}$	∞	1.0000	∞	0	0	-0.2458	0	0
1	66.28	[a]1.1998	0.3255	.501	.0849	-.2152	6.4838	5.0200
2	57.80	[a]1.3457	.1560	1.006	.1055	-.1626	4.7171	1.2607
3	52.94	[a]1.3765	.0588	1.520	.1140	-.1285	3.3077	.6595
4	49.44	1.3710	-.0112	2.047	.1181	-.1037	2.4177	.2982
5	46.71	1.3692	-.0658	2.593	.1200	-.0830	1.8974	.0902
6	44.39	1.3742	-.1122	3.164	.1203	-.0662	1.5696	.0308
7	42.35	1.3647	-.1530	3.766	.1204	-.0515	1.2936	-.0036
8	40.50	1.3537	-.1901	4.408	.1202	-.0385	1.0805	-.0315
9	38.78	1.3443	-.2244	5.101	.1199	-.0263	.9154	-.0426
10	37.16	1.3501	-.2568	5.857	.1193	-.0148	.8074	-.0521
11	35.60	1.3446	-.2880	6.692	.1185	-.0036	.6985	-.0579
12	34.06	1.3484	-.3188	7.628	.1174	.0072	.6185	-.0768
13	32.52	1.3525	-.3496	8.694	.1160	.0180	.5477	-.0813
14	30.94	1.3439	-.3811	9.931	.1143	.0287	.4710	-.0773
15	29.31	1.3340	-.4138	11.396	.1123	.0397	.4017	-.0739
16	27.58	1.3216	-.4485	13.174	.1100	.0510	.3386	-.0813
17	25.70	1.3118	-.4860	15.398	.1070	.0629	.2830	-.0750
18	23.62	1.2931	-.5275	18.286	.1036	.0757	.2272	-.0676
19	21.26	1.2871	-.5749	22.222	.0990	.0898	.1838	-.0620
20	18.46	1.2642	-.6309	27.943	.0939	.1055	.1368	-.0560
21	15.00	1.2476	-.7001	37.058	.0849	.1237	.0974	-.0485
22	10.52	1.2381	-.7896	53.714	.0722	.1462	.0636	-.0399
23	4.645	1.1758	-.9071	90.974	.0500	.1740	.0271	-.0314
24	0	0	-1.0000	180.000	0	.1887	0	-.0344
	Rear half of airfoil							
$0 \times 7\frac{1}{2}$	-∞	1.0000	∞	0	0	-0.2660	0	0
1	29.70	[a]1.3950	0.4061	.501	.1127	-.2194	10.3834	1.9169
2	37.16	[a]1.3927	.2567	1.006	.1192	-.1468	5.1175	.3331
3	41.90	[a]1.3449	.1621	1.520	.1204	-.1100	3.0781	.0306
4	45.42	1.3684	.0916	2.047	.1201	-.0857	2.3995	-.0963
5	48.14	1.3756	.0372	2.593	.1192	-.0649	1.9233	-.1709
6	50.47	1.3689	-.0094	3.164	.1171	-.0481	1.5591	-.2245
7	52.50	1.3469	-.0499	3.766	.1147	-.0332	1.2544	-.2347
8	54.36	1.3365	-.0872	4.408	.1119	-.0204	1.0506	-.2437
9	56.09	1.3193	-.1218	5.101	.1089	-.0085	.8769	-.2580
10	57.76	1.3013	-.1551	5.857	.1054	.0021	.7338	-.2531
11	59.38	1.2876	-.1875	6.692	.1020	.0121	.6218	-.2409
12	61.00	1.2764	-.2199	7.628	.0981	.0213	.5303	-.2237
13	62.63	1.2499	-.2526	8.694	.0942	.0302	.4312	-.2048
14	64.32	1.2362	-.2863	9.931	.0900	.0387	.3618	-.1864
15	66.08	1.2182	-.3215	11.396	.0854	.0472	.2965	-.1677
16	67.96	1.2010	-.3592	13.174	.0805	.0555	.2415	-.1569
17	70.01	1.1830	-.4002	15.398	.0748	.0639	.1919	-.1388
18	72.32	1.1624	-.4464	18.286	.0684	.0720	.1459	-.1148
19	74.96	1.1336	-.4992	22.222	.0613	.0806	.1024	-.0988
20	78.13	1.1045	-.5626	27.943	.0523	.0890	.0662	-.0813
21	82.10	1.0737	-.6420	37.058	.0413	.0971	.0364	-.0578
22	87.38	1.0321	-.7476	53.714	.0278	.1034	.0120	-.0367
23	94.57	.9826	-.8914	90.974	.0111	.1049	-.0018	-.0173
24	100.00	0	-1.0000	180.000	0	.1039	0	0

[a]Rejected points.

488

TABLE III. - VELOCITY DISTRIBUTIONS AND CARTESIAN MAPPING FUNCTIONS FOR 24-PERCENT-THICK AIRFOIL

(a) c/h, 0; method of finite chord; r, 1.1855; τ, 0.0317

φ (deg)	Percent chord	$\frac{v_i}{V}$	x	Δy	Δx	$\frac{d\Delta x}{d\varphi}$	$\frac{d\Delta y}{d\varphi}$
0 × 15	0	0	1.0000	0	-0.2172	0	0.2103
1	1.720	.9233	.9656	.0542	-.2112	.0460	.2059
2	6.735	1.1013	.8653	.1067	-.1931	.0922	.1977
3	14.64	1.1634	.7071	.1564	-.1629	.1412	.1825
4	24.64	1.2297	.5071	.2002	-.1173	.2055	.1509
5	35.84	1.2962	.2832	.2314	-.0553	.2654	.0818
6	47.42	1.3361	.0517	.2388	.0200	.2986	-.0267
7	59.10	1.2682	-.1820	.2164	.0931	.2531	-.1400
8	70.60	1.1594	-.4119	.1683	.1491	.1682	-.2174
9	81.49	1.0178	-.6298	.1078	.1768	.0477	-.2308
10	90.92	.9019	-.8184	.0536	.1766	-.0406	-.1756
11	97.54	.8217	-.9508	.0188	.1626	-.0546	-.0939
12	100.00	0	-1.0000	0	.1538	0	-.0569

(b) c/h, 0.5; method of finite chord; cosh k, 1.34708; τ, 0.05243

φ (deg)	Percent chord	$\frac{v_c}{V}$	$\frac{x}{0.5\pi}$	$\frac{\Delta y}{0.5\pi}$	Δx	$\frac{d\Delta x}{d\varphi}$	$\frac{d\Delta y}{d\varphi}$
0 × 15	0	0	1.0000	0	-0.3930	0	0.4310
1	2.855	1.0375	.9429	.0705	-.3744	.1396	.3961
2	10.14	1.1600	.7972	.1302	-.3263	.2248	.3276
3	19.42	1.2225	.6115	.1787	-.2581	.2918	.2566
4	29.04	1.2954	.4193	.2151	-.1733	.3530	.1721
5	38.38	1.3442	.2325	.2353	-.0763	.3837	.0719
6	47.50	1.3602	.0500	.2386	.0261	.3938	-.0362
7	56.68	1.2302	-.1335	.2232	.1270	.3713	-.1506
8	66.24	1.2304	-.3248	.1888	.2169	.3085	-.2645
9	76.46	1.1082	-.5291	.1370	.2826	.1893	-.3504
10	87.08	.9768	-.7415	.0757	.3090	.0157	-.3411
11	96.20	.8790	-.9240	.0262	.2992	-.0807	-.2236
12	100.00	0	-1.0000	0	.2882	0	-.1468

TABLE II. - VELOCITY DISTRIBUTIONS AND CARTESIAN MAPPING

FUNCTIONS FOR 24-PERCENT-THICK AIRFOIL - Continued

(c) c/h, 1.0; method of semi-infinite chord; c, 2; h, 2; n, 6

θ (deg)	Percent chord	$\frac{v_c}{V}$	x	φ (deg)	Δy	Δx	$\frac{d\Delta x}{d\varphi}$	$\frac{d\Delta y}{d\varphi}$
Front half of airfoil								
0 × 7$\frac{1}{2}$	∞	1.0000	∞	0	0	-0.2370	0	0
1	115.6	[a].9661	1.3125	1.252	0	-.2574	-1.0231	0
2	92.24	[a].8895	.8449	2.514	.0471	-.2811	-1.0200	4.9886
3	79.28	[a]1.1239	.5856	3.798	.1221	-.2778	1.4057	2.4101
4	71.70	[a]1.2656	.4340	5.114	.1640	-.2400	1.6663	1.3743
5	66.07	1.3231	.3214	6.476	.1899	-.2025	1.4736	.9146
6	61.44	1.3662	.2289	7.898	.2081	-.1687	1.2873	.5854
7	57.54	1.4146	.1509	9.397	.2208	-.1363	1.1610	.3766
8	54.09	1.4469	.0818	10.993	.2297	-.1059	1.0337	.2339
9	50.94	1.4652	.0188	12.709	.2350	-.0768	.9129	.1458
10	47.98	1.4733	-.0405	14.576	.2383	-.0493	.8010	.0684
11	45.14	1.4769	-.0971	16.631	.2396	-.0224	.7032	.0104
12	42.37	1.4745	-.1526	18.925	.2389	.0037	.6148	-.0277
13	39.60	1.4674	-.2079	21.521	.2368	.0294	.5351	-.0608
14	36.80	1.4554	-.2640	24.509	.2330	.0549	.4620	-.0827
15	33.91	1.4346	-.3218	28.012	.2276	.0806	.3921	-.0984
16	30.87	1.4059	-.3826	32.204	.2201	.1066	.3258	-.1078
17	27.62	1.3730	-.4475	37.347	.2104	.1332	.2651	-.1121
18	24.10	1.3468	-.5180	43.837	.1980	.1603	.2142	-.1102
19	20.20	1.3152	-.5961	52.301	.1819	.1880	.1669	-.1060
20	15.85	1.2832	-.6830	63.764	.1621	.2163	.1246	-.0958
21	11.09	1.2482	-.7782	79.919	.1365	.2456	.0879	-.0858
22	6.130	1.1717	-.8774	103.388	.1018	.2739	.0526	-.0806
23	1.835	1.0333	-.9633	137.064	.0561	.2966	.0306	-.0758
24	0	0	-1.0000	180.000	0	.3056	0	-.0738
Rear half of airfoil								
0 × 7$\frac{1}{2}$	-∞	1.0000	∞	0	0	-0.2733	0	0
1	-17.43	[a].9558	1.3486	1.252	0	-.3040	-1.3465	0
2	5.740	[a].9243	.8852	2.514	.1001	-.3234	0	5.9909
3	16.71	[a]1.3396	.6658	3.798	.1677	-.2803	2.6010	1.5367
4	23.56	[a]1.3535	.5287	5.114	.1959	-.2281	1.9476	.9475
5	29.04	[a]1.3767	.4193	6.476	.2144	-.1872	1.5893	.6356
6	33.48	[a]1.4015	.3303	7.898	.2264	-.1500	1.3419	.3701
7	37.32	[a]1.4374	.2537	9.397	.2338	-.1162	1.1847	.1831
8	40.72	[a]1.4570	.1856	10.993	.2378	-.0848	1.0391	.0856
9	43.86	[a]1.4662	.1227	12.709	.2395	-.0556	.9090	.0225
10	46.81	[a]1.4634	.0638	14.576	.2391	-.0276	.7888	-.0406
11	49.65	1.4686	.0070	16.631	.2368	-.0010	.6973	-.0843
12	52.44	1.4596	-.0487	18.925	.2328	.0249	.6066	-.1162
13	55.22	1.4439	-.1045	21.521	.2272	.0501	.5230	-.1371
14	58.06	1.4202	-.1612	24.509	.2197	.0751	.4447	-.1512
15	61.01	1.3814	-.2202	28.012	.2100	.0996	.3679	-.1690
16	64.13	1.3430	-.2826	32.204	.1982	.1239	.2984	-.1653
17	67.50	1.3070	-.3501	37.347	.1833	.1478	.2398	-.1626
18	71.21	1.2558	-.4242	43.837	.1656	.1714	.1817	-.1594
19	75.38	1.1933	-.5076	52.301	.1429	.1937	.1250	-.1462
20	80.18	1.1161	-.6036	63.764	.1153	.2130	.0715	-.1282
21	85.72	1.0334	-.7145	79.919	.0832	.2265	.0257	-.0985
22	91.88	.9658	-.8377	103.388	.0480	.2309	0	-.0675
23	97.54	.8979	-.9507	137.064	.0189	.2265	-.0092	-.0371
24	100.00	0	-1.0000	180.000	0	.2230	0	0

[a]Rejected points.

NACA

TABLE III. - VELOCITY DISTRIBUTIONS AND CARTESIAN MAPPING

FUNCTIONS FOR 24-PERCENT-THICK AIRFOIL - Continued

(d) c/h, 1.5; method of semi-infinite chord; c, 2; h, 4/3; n, 8

θ (deg)	Percent chord	$\frac{V_c}{V}$	x	φ (deg)	Δy	Δx	$\frac{d\Delta x}{d\varphi}$	$\frac{d\Delta y}{d\varphi}$
Front half of airfoil								
$0 \times 7\frac{1}{2}$	∞	1.0000	∞	0	0	-0.4634	0	0
1	74.50	[a]1.2438	0.4900	.626	.1477	-.4140	8.7854	8.4772
2	63.92	[a]1.5358	.2784	1.257	.1997	-.3236	7.0656	2.8107
3	58.32	[a]1.5987	.1664	1.899	.2189	-.2569	4.8956	1.2701
4	54.29	[a]1.6524	.0858	2.558	.2292	-.2086	3.7931	.6855
5	51.17	[a]1.6718	.0234	3.241	.2348	-.1686	3.0286	.3554
6	48.56	[a]1.6763	-.0289	3.954	.2379	-.1348	2.4837	.1598
7	46.29	1.6684	-.0742	4.706	.2393	-.1046	2.0691	.0510
8	44.23	1.6617	-.1154	5.509	.2395	-.0776	1.7564	-.0144
9	42.34	1.6654	-.1533	6.374	.2389	-.0525	1.5237	-.0673
10	40.52	1.6613	-.1896	7.318	.2375	-.0290	1.3234	-.0986
11	38.76	1.6633	-.2247	8.360	.2356	-.0065	1.1618	-.1159
12	37.04	1.6600	-.2593	9.527	.2334	.0154	1.0180	-.1299
13	35.30	1.6441	-.2939	10.856	.2303	.0371	.8818	-.1369
14	33.53	1.6197	-.3294	12.396	.2267	.0589	.7562	-.1436
15	31.68	1.6023	-.3664	14.218	.2221	.0810	.6494	-.1441
16	29.71	1.5813	-.4058	16.426	.2168	.1038	.5515	-.1426
17	27.57	1.5582	-.4486	19.183	.2102	.1276	.4619	-.1388
18	25.20	1.5281	-.4960	22.750	.2022	.1532	.3769	-.1304
19	22.48	1.4856	-.5505	27.586	.1916	.1809	.2953	-.1209
20	19.24	1.4333	-.6151	34.552	.1777	.2114	.2182	-.1058
21	15.27	1.3815	-.6946	45.462	.1590	.2459	.1513	-.0907
22	10.26	1.3382	-.7949	64.666	.1309	.2864	.0962	-.0750
23	4.130	1.2114	-.9174	103.629	.0840	.3306	.0444	-.0631
24	0	0	-1.0000	180.000	0	.3524	0	-.0664
Rear half of airfoil								
$0 \times 7\frac{1}{2}$	$-\infty$	1.0000	∞	0	0	-0.5031	0	0
1	21.64	[a]1.4721	0.5672	.626	.1879	-.4314	13.2430	6.3899
2	30.83	[a]1.7148	.3834	1.257	.2200	-.3132	8.1650	1.5171
3	36.26	[a]1.6763	.2749	1.899	.2320	-.2431	5.1959	.6839
4	40.26	[a]1.6823	.1948	2.558	.2372	-.1942	3.8646	.3391
5	43.32	[a]1.6921	.1335	3.241	.2394	-.1530	3.0691	.0925
6	45.94	1.6674	.0812	3.954	.2394	-.1192	2.4612	-.0549
7	48.19	1.6621	.0362	4.706	.2382	-.0889	2.0595	-.1218
8	50.26	1.6608	-.0053	5.509	.2361	-.0622	1.7591	-.1478
9	52.18	1.6477	-.0435	6.374	.2333	-.0373	1.5062	-.1939
10	54.02	1.6361	-.0803	7.318	.2300	-.0143	1.3015	-.2123
11	55.78	1.6222	-.1155	8.360	.2261	.0080	1.1275	-.2216
12	57.54	1.6049	-.1507	9.527	.2213	.0293	.9759	-.2254
13	59.30	1.5798	-.1861	10.856	.2160	.0503	.8382	-.2285
14	61.14	1.5539	-.2228	12.396	.2097	.0709	.7170	-.2263
15	63.05	1.5252	-.2610	14.218	.2027	.0918	.6086	-.2238
16	65.10	1.4869	-.3021	16.426	.1943	.1129	.5056	-.2174
17	67.34	1.4427	-.3468	19.183	.1843	.1347	.4105	-.2076
18	69.87	1.3967	-.3974	22.750	.1723	.1572	.3239	-.1900
19	72.78	1.3566	-.4557	27.586	.1572	.1811	.2507	-.1714
20	76.32	1.2716	-.5265	34.552	.1376	.2054	.1662	-.1468
21	80.80	1.1723	-.6160	45.462	.1117	.2299	.0916	-.1205
22	86.82	1.0763	-.7365	64.666	.0770	.2502	.0360	-.0863
23	94.77	.9593	-.8954	103.629	.0333	.2580	0	-.0491
24	100.00	0	-1.0000	180.000	0	.2577	0	0

[a]Rejected points.

NACA

TABLE III. - VELOCITY DISTRIBUTIONS AND CARTESIAN MAPPING

FUNCTIONS FOR 24-PERCENT-THICK AIRFOIL - Concluded

(e) c/h, 2.0; method of semi-infinite chord; c, 2; h, 1; n, 30

θ (deg)	Percent chord	$\frac{v_c}{V}$	x	φ (deg)	Δy	Δx	$\frac{d\Delta x}{d\varphi}$	$\frac{d\Delta y}{d\varphi}$
Front half of airfoil								
0 × 7½	∞	1.0000	∞	0	0	-0.5528	0	0
1	54.02	[a]2.9318	0.0805	.250	.2298	-.4566	48.0667	1.9118
2	50.26	[a]2.4921	.0053	.503	.2361	-.3098	21.7485	1.0144
3	47.18	2.0095	-.0564	.760	.2389	-.2401	12.0661	.4444
4	44.74	2.0103	-.1052	1.024	.2396	-.1941	8.9548	.0168
5	42.93	2.0025	-.1414	1.297	.2391	-.1550	7.0434	-.1671
6	41.30	1.9859	-.1739	1.582	.2381	-.1242	5.7267	-.2203
7	39.94	1.9569	-.2012	1.884	.2370	-.0960	4.7407	-.2510
8	38.65	1.9564	-.2270	2.205	.2355	-.0716	4.0515	-.2701
9	37.48	1.9472	-.2503	2.552	.2340	-.0485	3.4861	-.2747
10	36.35	1.9430	-.2730	2.930	.2322	-.0272	3.0307	-.2645
11	35.27	1.9505	-.2946	3.349	.2303	-.0063	2.6647	-.2546
12	34.18	1.9379	-.3165	3.818	.2280	.0136	2.3231	-.2463
13	33.09	1.9070	-.3382	4.354	.2258	.0336	2.0049	-.2429
14	31.97	1.8601	-.3606	4.975	.2230	.0536	1.7098	-.2479
15	30.80	1.8257	-.3840	5.712	.2200	.0742	1.4593	-.2395
16	29.55	1.8080	-.4090	6.609	.2166	.0956	1.2492	-.2288
17	28.19	1.7828	-.4362	7.734	.2123	.1184	1.0517	-.2164
18	26.66	1.7531	-.4667	9.202	.2074	.1431	.8667	-.1959
19	24.88	1.7156	-.5023	11.217	.2010	.1704	.6916	-.1709
20	22.76	1.6762	-.5448	14.182	.1928	.2022	.5312	-.1510
21	19.97	1.6100	-.6006	19.026	.1810	.2393	.3754	-.1347
22	16.14	1.5680	-.6771	28.416	.1632	.2887	.2396	-.0971
23	10.28	1.4955	-.7944	53.913	.1309	.3667	.1118	-.0576
24	0	0	-1.0000	180.000	0	.4129	0	-.1019
Rear half of airfoil								
0 × 7½	−∞	1.0000	∞	0	0	-0.5504	0	0
1	40.56	[a]6.4445	0.1887	.250	.2377	-.4492	61.6136	1.3365
2	44.00	[a]2.4479	.1199	.503	.2396	-.2960	21.4506	0
3	47.02	2.0071	.0597	.760	.2389	-.2249	12.0523	-.4346
4	49.48	1.9861	.0105	1.024	.2368	-.1793	8.8597	-.4759
5	51.30	1.9730	-.0260	1.297	.2345	-.1405	6.9538	-.5004
6	52.95	1.9658	-.0590	1.582	.2318	-.1102	5.6857	-.5122
7	54.34	1.9234	-.0869	1.884	.2290	-.0825	4.6755	-.5214
8	55.66	1.8777	-.1132	2.205	.2262	-.0588	3.8962	-.5177
9	56.86	1.8665	-.1372	2.552	.2229	-.0362	3.3512	-.5084
10	58.04	1.8667	-.1608	2.930	.2197	-.0158	2.9249	-.4875
11	59.16	1.8613	-.1833	3.349	.2162	.0042	2.5560	-.4616
12	60.31	1.8437	-.2062	3.818	.2126	.0230	2.2225	-.4400
13	61.44	1.8095	-.2289	4.354	.2086	.0421	1.9108	-.4153
14	62.64	1.7660	-.2528	4.975	.2041	.0606	1.6263	-.3910
15	63.88	1.7268	-.2776	5.712	.1994	.0798	1.3804	-.3713
16	65.21	1.6881	-.3042	6.609	.1940	.0995	1.1604	-.3446
17	66.67	1.6515	-.3334	7.734	.1873	.1203	.9645	-.3166
18	68.34	1.6074	-.3667	9.202	.1797	.1422	.7827	-.2932
19	70.27	1.5614	-.4054	11.217	.1701	.1664	.6165	-.2629
20	72.65	1.5014	-.4530	14.182	.1580	.1931	.4565	-.2214
21	75.74	1.4235	-.5147	19.026	.1410	.2243	.3065	-.1772
22	80.21	1.2813	-.6042	28.416	.1150	.2607	.1560	-.1318
23	88.20	1.0860	-.7639	53.913	.0690	.2963	.0362	-.0803
24	100.00	0	-1.0000	180.000	0	.3120	0	0

[a]Rejected points.

NACA

TABLE IV. - LOCAL CONSTRICTION CORRECTIONS $\Delta v/V$ FOR 12-PERCENT-THICK AIRFOIL

Percent chord	Conformal-mapping correction				First-order image correction				Percent chord	Second-order image correction			
	c/h				c/h					c/h			
	0.5	1.0	1.5	2.0	0.5	1.0	1.5	2.0		0.5	1.0	1.5	2.0
0	0	0	0	0	0	0	0	0	0	0	0	0	0
5.0	.020	.058	.085	.118	.0124	.0516	.1193	.2183	.7595	.0094	.0249	.0029	-.1475
10.0	.012	.040	.075	.137	.0128	.0529	.1224	.2240	3.016	.0098	.0277	.0140	-.1141
15.0	.009	.038	.080	.133	.0129	.0536	.1241	.2270	6.698	.0103	.0316	.0315	-.0584
20.0	.010	.043	.091	.151	.0130	.0540	.1250	.2286	11.70	.0108	.0362	.0534	.0130
25.0	.014	.050	.103	.173	.0131	.0544	.1260	.2305	17.86	.0111	.0409	.0764	.0899
30.0	.013	.055	.112	.193	.0133	.0550	.1272	.2327	25.00	.0115	.0451	.0978	.1611
35.0	.010	.053	.116	.194	.0134	.0556	.1287	.2354	32.90	.0118	.0488	.1152	.2180
40.0	.008	.047	.102	.182	.0135	.0562	.1300	.2378	41.32	.0122	.0513	.1259	.2514
45.0	.011	.048	.104	.199	.0136	.0563	.1303	.2384	50.00	.0121	.0510	.1250	.2493
50.0	.016	.055	.121	.204	.0135	.0560	.1297	.2372	58.68	.0116	.0478	.1120	.2099
55.0	.018	.054	.113	.183	.0133	.0552	.1277	.2335	67.10	.0109	.0422	.0896	.1419
60.0	.014	.047	.099	.160	.0130	.0539	.1247	.2280	75.00	.0101	.0362	.0634	.0601
65.0	.014	.043	.088	.145	.0126	.0523	.1210	.2213	82.14	.0095	.0302	.0363	-.0270
70.0	.014	.040	.080	.128	.0122	.0507	.1174	.2148	88.30	.0089	.0247	.0103	-.1117
75.0	.014	.038	.073	.112	.0119	.0492	.1139	.2083	93.30	.0084	.0198	-.0124	-.1852
80.0	.012	.033	.062	.093	.0116	.0480	.1110	.2030	96.98	.0080	.0159	-.0297	-.2405
85.0	.010	.027	.049	.075	.0113	.0469	.1085	.1985	-------	------	------	------	------
90.0	.005	.030	.042	.061	.0110	.0457	.1057	.1934	-------	------	------	------	------
95.0	.009	.041	.045	.059	.0107	.0443	.1025	.1875	-------	------	------	------	------

TABLE V. - LOCAL CONSTRICTION CORRECTIONS $\Delta v/V$ FOR 24-PERCENT-THICK AIRFOILS

Percent chord	Conformal-mapping correction				First-order image correction				Percent chord	Second-order image correction			
	c/h				c/h					c/h			
	0.5	1.0	1.5	2.0	0.5	1.0	1.5	2.0		0.5	1.0	1.5	2.0
0	0	0	0	0	0	0	0	0	0	0	0	0	0
5.0	.030	.067	.175	-----	.0291	.1251	.3057	.5859	.7595	.0136	.0303	-.0429	-.4470
10.0	.029	.108	.206	.363	.0306	.1314	.3211	.6153	3.016	.0190	.0467	-.0293	-.5020
15.0	.027	.113	.214	.386	.0316	.1356	.3313	.6349	6.698	.0211	.0593	.0170	-.3633
20.0	.028	.115	.245	.430	.0325	.1397	.3413	.6540	11.70	.0225	.0724	.0794	-.1458
25.0	.033	.122	.289	.488	.0334	.1434	.3504	.6714	17.86	.0241	.0871	.1501	.1012
30.0	.038	.136	.323	.558	.0342	.1469	.3589	.6878	25.00	.0257	.1020	.2212	.3482
35.0	.038	.150	.348	.650	.0350	.1503	.3672	.7036	32.90	.0272	.1153	.2831	.5612
40.0	.032	.151	.347	.645	.0357	.1534	.3748	.7183	41.32	.0286	.1254	.3268	.7067
45.0	.024	.140	.330	.675	.0362	.1555	.3800	.7281	50.00	.0287	.1268	.3344	.7341
50.0	.029	.144	.334	.656	.0359	.1543	.3771	.7227	58.68	.0273	.1179	.3002	.6282
55.0	.034	.146	.331	.596	.0352	.1512	.3694	.7080	67.10	.0252	.1034	.2398	.4322
60.0	.032	.138	.311	.590	.0341	.1467	.3583	.6867	75.00	.0227	.0856	.1650	.1877
65.0	.027	.122	.275	.480	.0329	.1414	.3455	.6622	82.14	.0201	.0673	.0887	-.0602
70.0	.020	.105	.230	.404	.0316	.1356	.3313	.6349	88.30	.0180	.0516	.0218	-.2804
75.0	.020	.091	.194	.335	.0299	.1286	.3143	.6022	93.30	.0163	.0390	-.0322	-.4591
80.0	.023	.082	.163	.265	.0281	.1208	.2952	.5657	96.98	.0150	.0299	-.0709	-.5858
85.0	.030	.077	.137	.194	.0263	.1131	.2764	.5297	-------	------	------	------	------
90.0	.031	.072	.116	.135	.0247	.1062	.2594	.4970	-------	------	------	------	------
95.0	.037	.074	.103	-----	.0231	.0992	.2423	.4643	-------	------	------	------	------

NACA

TABLE VI. - AVERAGE CONSTRICTION CORRECTIONS

Method	c/h	12-percent-thick airfoil	24-percent-thick airfoil	10-percent Kaplan section
Conformal-mapping correction	0.5	0.0123	0.0294	0.0085
	1.0	.0444	.1199	.0305
	1.5	.0907	.2642	----------
	2.0	.1511	.4731	.1033
First-order image correction	0.5	0.0131	0.0324	----------
	1.0	.0534	.1397	----------
	1.5	.1226	.3406	----------
	2.0	.2250	.6538	----------
Second-order image correction	0.5	0.0110	0.0252	----------
	1.0	.0426	.0994	----------
	1.5	.0877	.2186	----------
	2.0	.1330	.3555	----------

TABLE VII. - CONJUGATE AND DERIVATIVE COEFFICIENTS FOR 24-POINT SCHEME

k	Conjugate coefficients a_k	Derivative coefficients b_k	k	Conjugate coefficients a_k	Derivative coefficients b_k
0	0	-4.95445	12	0	0.02778
1	-.42564	1.63040	13	.00366	.01413
2	-.20734	.41467	14	.01489	.02977
3	-.06706	.09484	15	.01151	.01627
4	-.09623	.11111	16	.03208	.03704
5	-.03620	.03748	17	.02131	.02207
6	-.05556	.05556	18	.05556	.05556
7	-.02131	.02207	19	.03620	.03748
8	-.03208	.03704	20	.09623	.11111
9	-.01151	.01627	21	.06706	.09484
10	-.01489	.02977	22	.20734	.41467
11	-.00366	.01413	23	.42564	1.63040

TABLE VIII. - CONJUGATE AND DERIVATIVE COEFFICIENTS

FOR 48-POINT SCHEME

k	Conjugate coefficients a_k	Derivative coefficients b_k	k	Conjugate coefficients a_k	Derivative coefficients b_k
0	0	-9.90891	24	0	0.01389
1	-.42470	3.24694	25	.00091	.00697
2	-.21099	.81517	26	.00366	.01413
3	-.06982	.18246	27	.00276	.00722
4	-.10367	.20733	28	.00744	.01489
5	-.04092	.06721	29	.00472	.00774
6	-.06706	.09484	30	.01151	.01627
7	-.02816	.03550	31	.00685	.00863
8	-.04811	.05556	32	.01604	.01852
9	-.02079	.02250	33	.00928	.01004
10	-.03620	.03748	34	.02132	.02207
11	-.01584	.01597	35	.01218	.01229
12	-.02778	.02778	36	.02778	.02778
13	-.01218	.01229	37	.01584	.01597
14	-.02132	.02207	38	.03620	.03748
15	-.00928	.01004	39	.02079	.02250
16	-.01604	.01852	40	.04811	.05556
17	-.00685	.00863	41	.02816	.03550
18	-.01151	.01627	42	.06706	.09484
19	-.00472	.00774	43	.04092	.06721
20	-.00744	.01489	44	.10367	.20733
21	-.00276	.00722	45	.06982	.18246
22	-.00366	.01413	46	.21099	.81517
23	-.00091	.00697	47	.42470	3.24694

TABLE IX. - CRITICAL MACH NUMBER OF ISOLATED AIRFOIL

[By equation (65), fig. 13, reference 7]

Method	t/h	c/h	$\frac{tc}{h^2}$	Critical Mach number: 12-percent-thick airfoil	Critical Mach number: 24-percent-thick airfoil
First-order image correction	0.06	0.5	0.03	0.74	0.63
	.12	1.0	.12	.75	.63
	.18	1.5	.27	.76	.65
	.24	2.0	.48	.78	.65
Second-order image correction	0.12	0.5	0.06	0.74	0.62
	.24	1.0	.24	.74	.61
	.36	1.5	.54	.75	.62
	.48	2.0	.96	.79	.68
Conformal-mapping correction-------------------				0.74	0.62

TABLE X. - CONSTANTS USED IN FIRST- AND SECOND-ORDER IMAGE CORRECTIONS

(a) Constants λ used in the first-order corrections

488

c/h	λ	
	12-percent-thick airfoil	24-percent-thick airfoil
0	3.89	2.24
.5	3.93	2.29
1.0	4.06	2.45
1.5	4.18	2.67
2.0	4.30	2.88

(b) Constants C_n used in second-order correction, c = 2

	C_n	
	12-percent-thick airfoil	24-percent-thick airfoil
C_0	0.08722	0.17157
C_1	.05534	.07177
C_2	-.02401	-.06306
C_3	.00455	.00158
C_4	.00475	-.00224

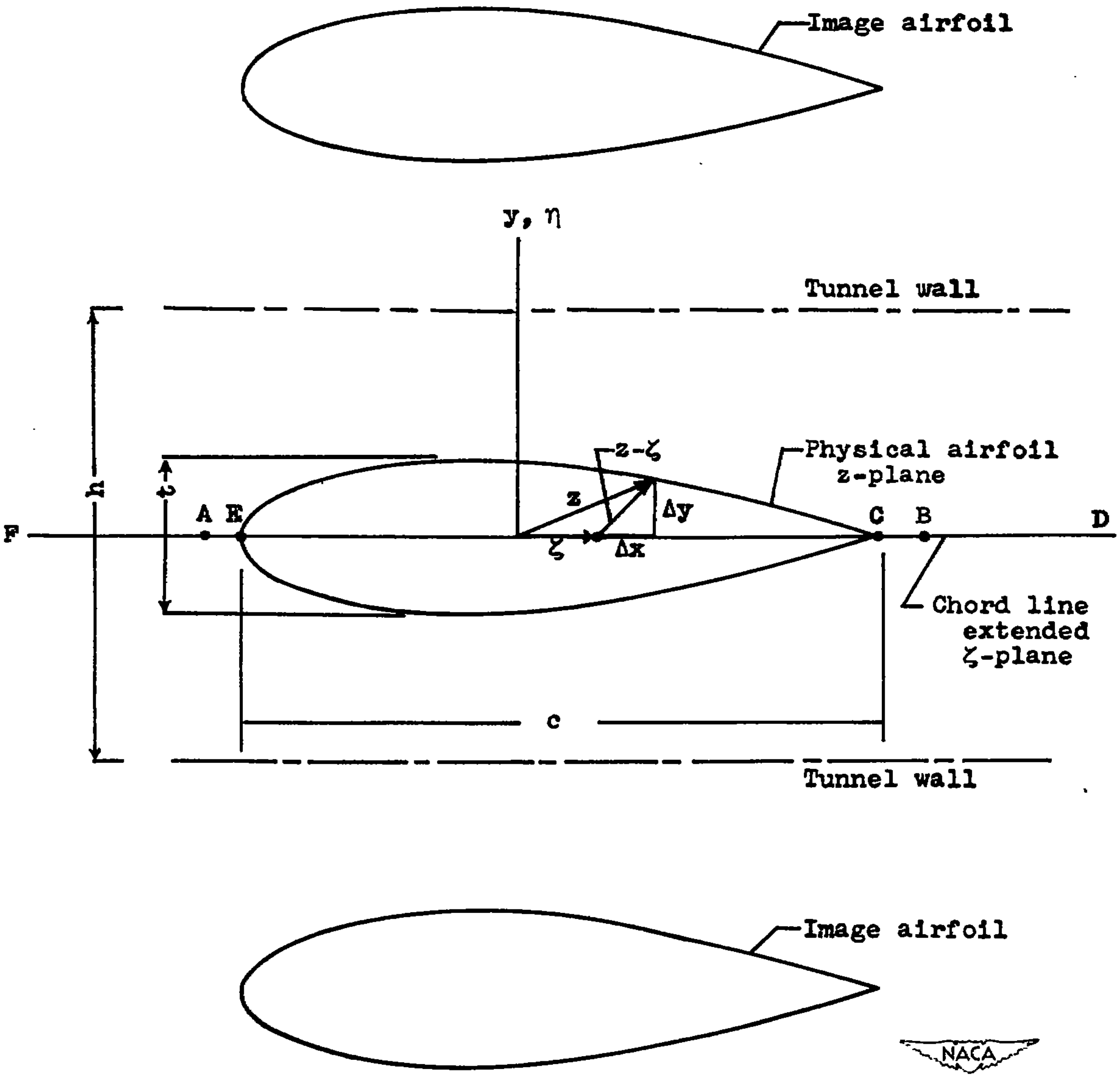

Figure 1.- Representation of symmetrical airfoil in two-dimensional tunnel as unstaggered cascade of airfoils; only three airfoils of cascade shown.

488

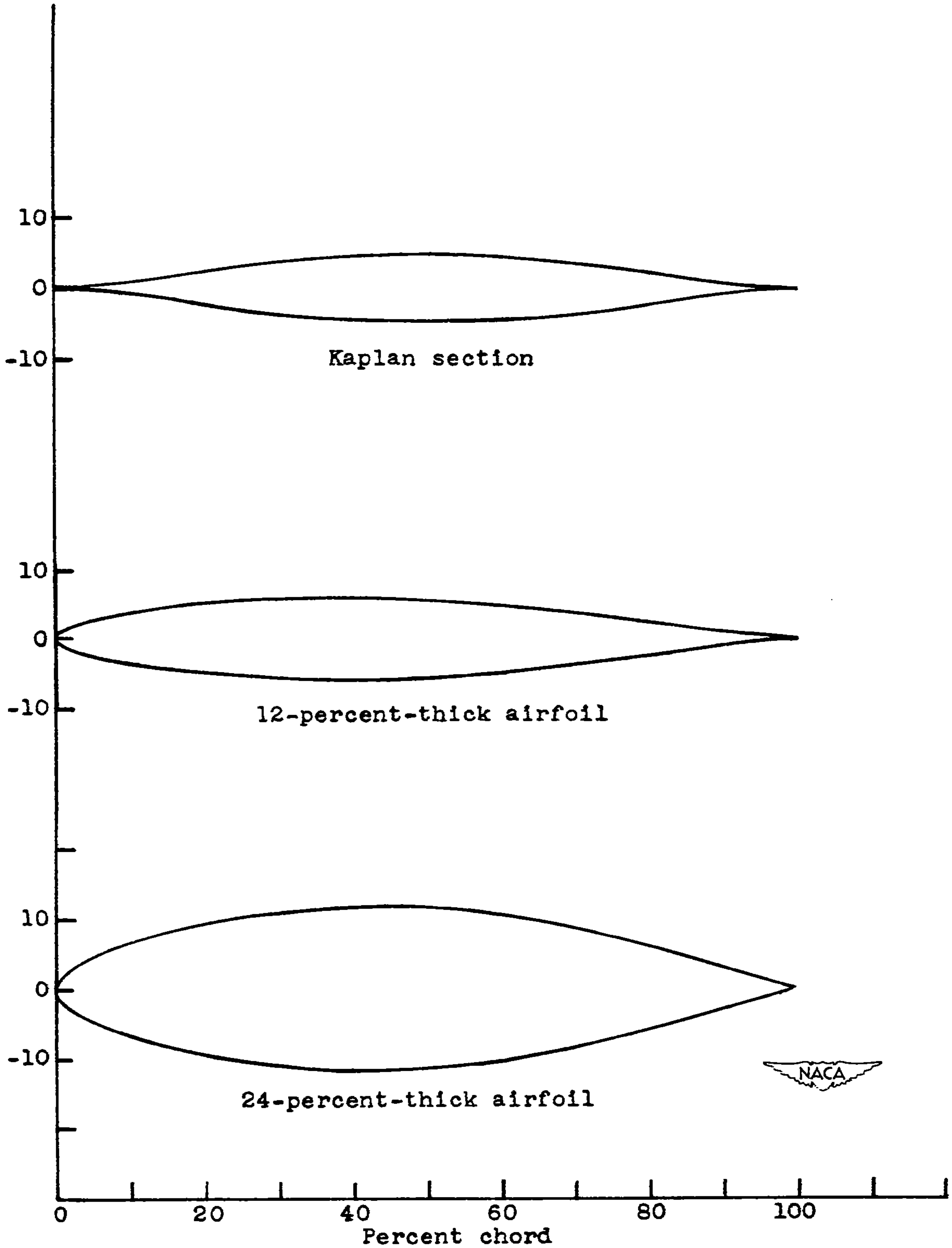

Figure 2.- Airfoil sections for which calculations were made.

488

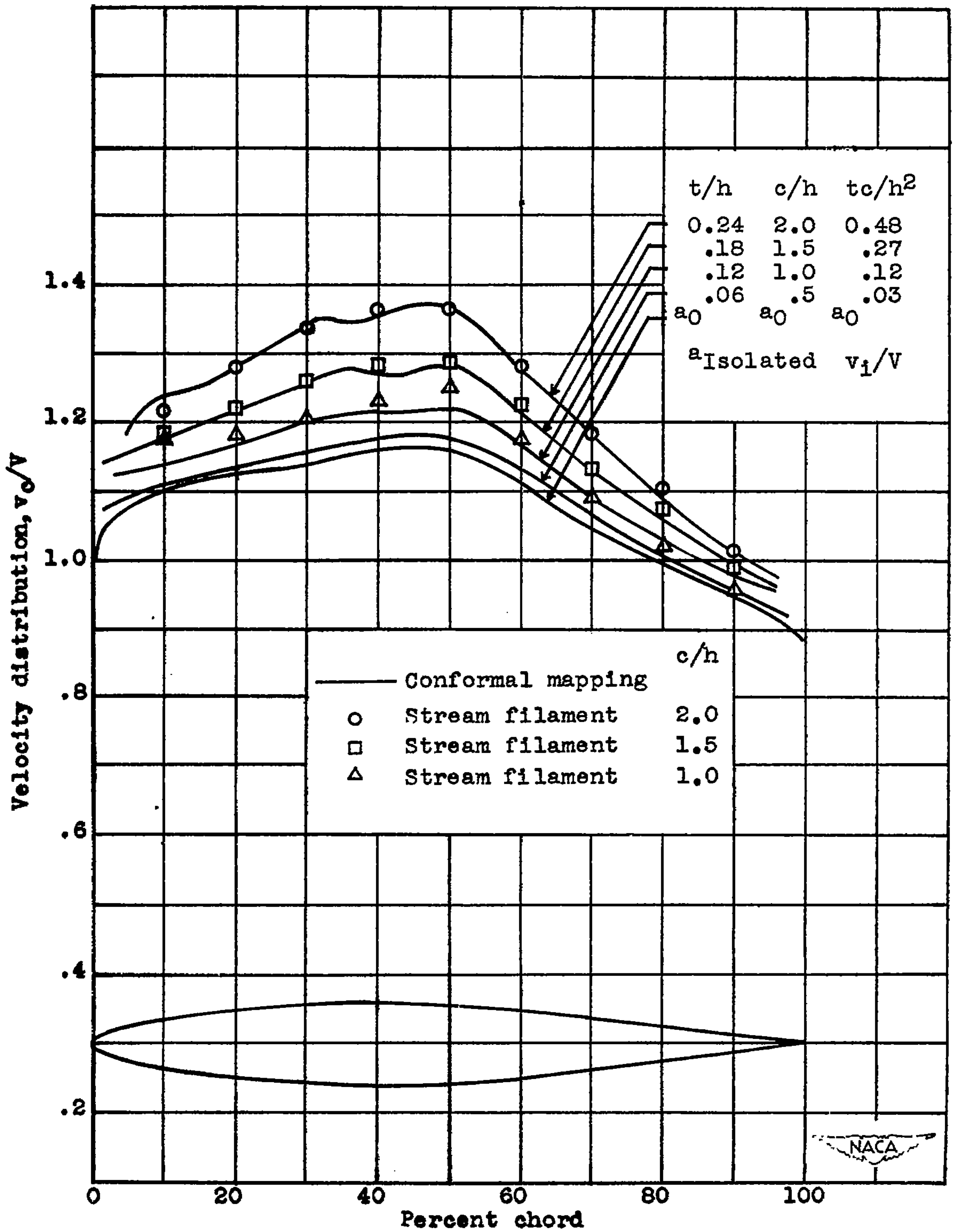

(a) 12-percent-thick airfoil.

Figure 3. - Velocity distributions on airfoils by mapping and stream-filament theory. c, chord of airfoil; h, height of tunnel; t, maximum thickness of airfoil.

488

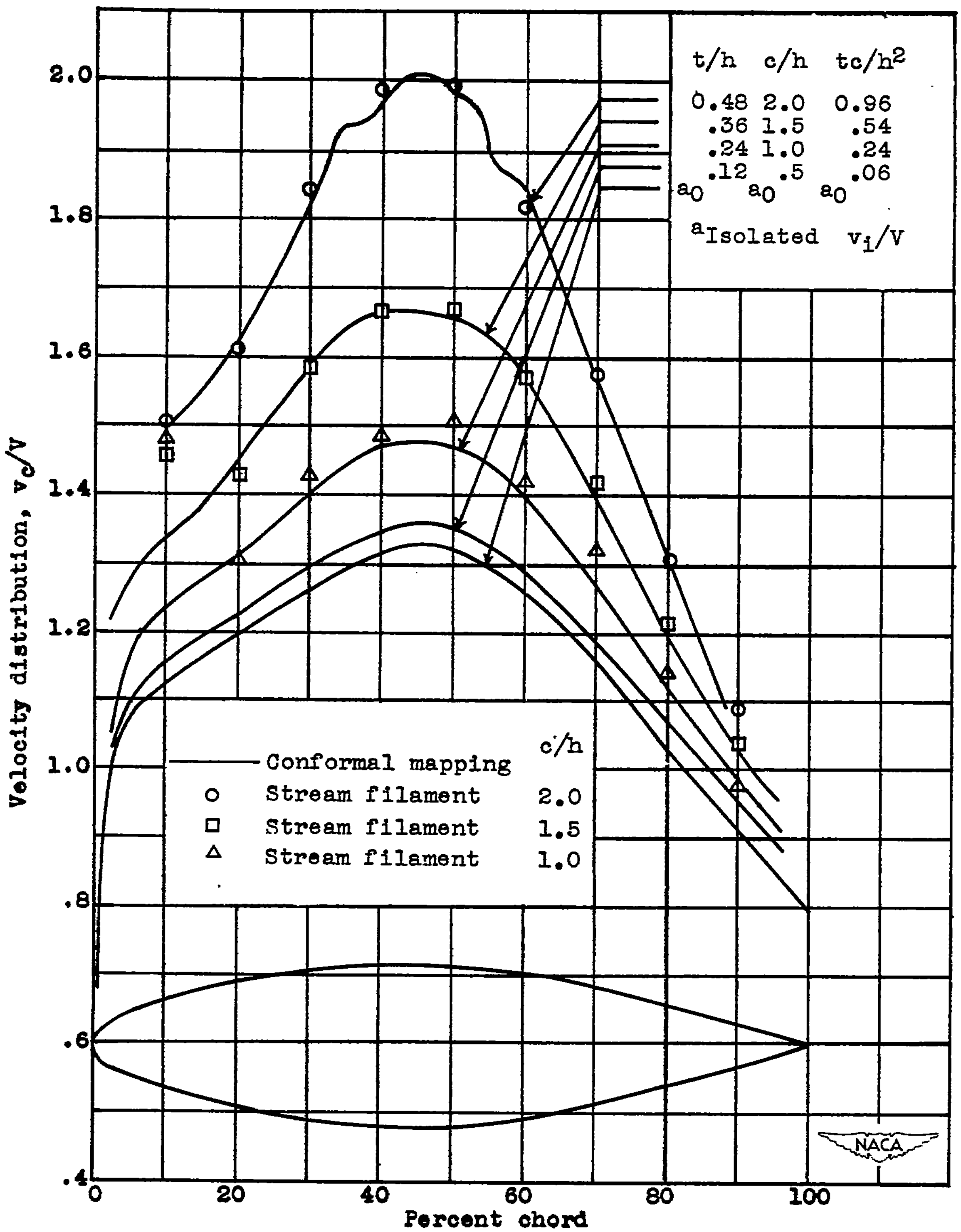

(b) 24-percent-thick airfoil.

Figure 3. - Concluded. Velocity distributions on airfoils by mapping and stream-filament theory. c, chord of airfoil; h, height of tunnel; t, maximum thickness of airfoil.

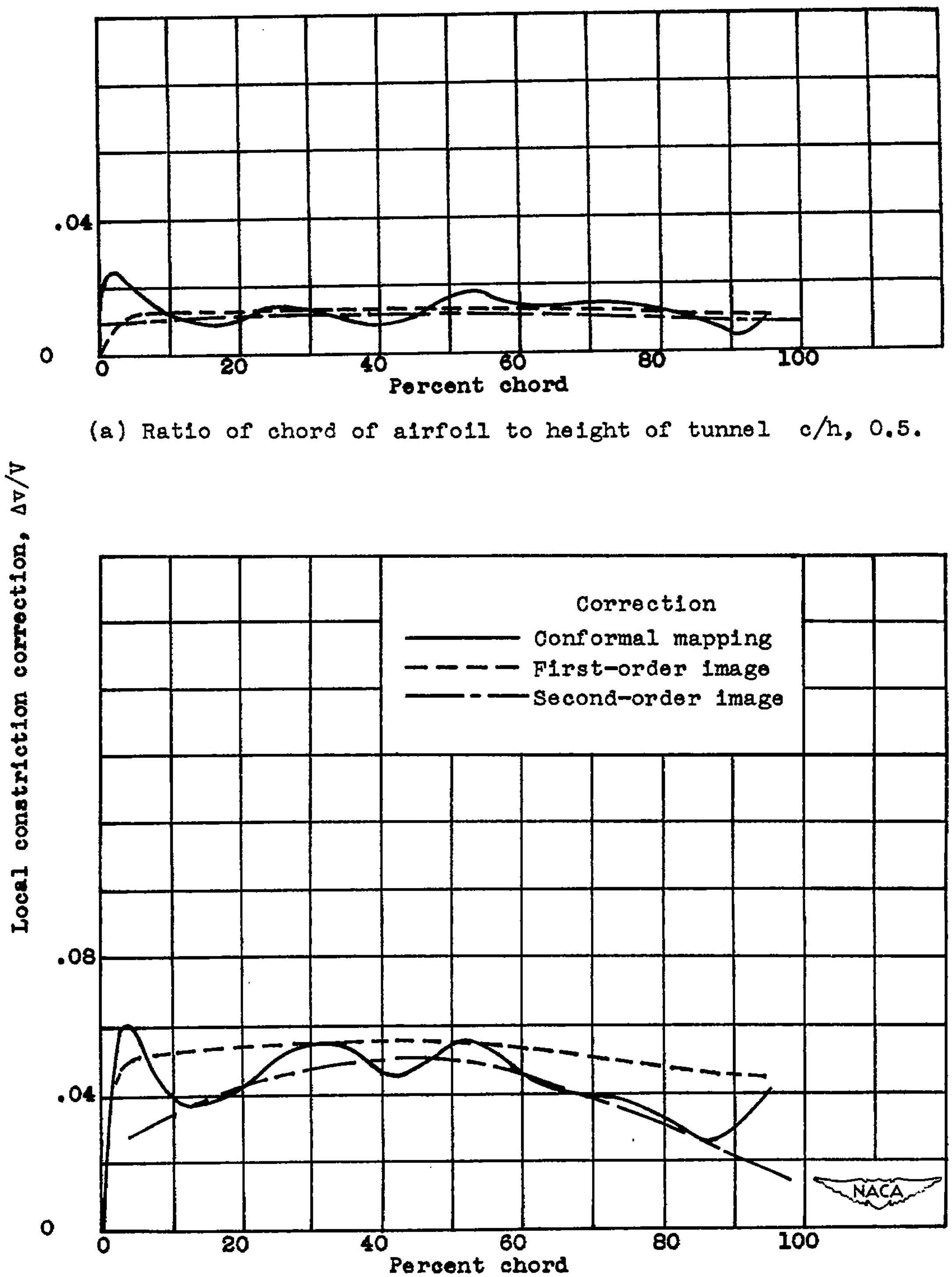

(a) Ratio of chord of airfoil to height of tunnel c/h, 0.5.

(b) Ratio of chord of airfoil to height of tunnel c/h, 1.0.

Figure 4. - Local constriction corrections for 12-percent-thick airfoil.

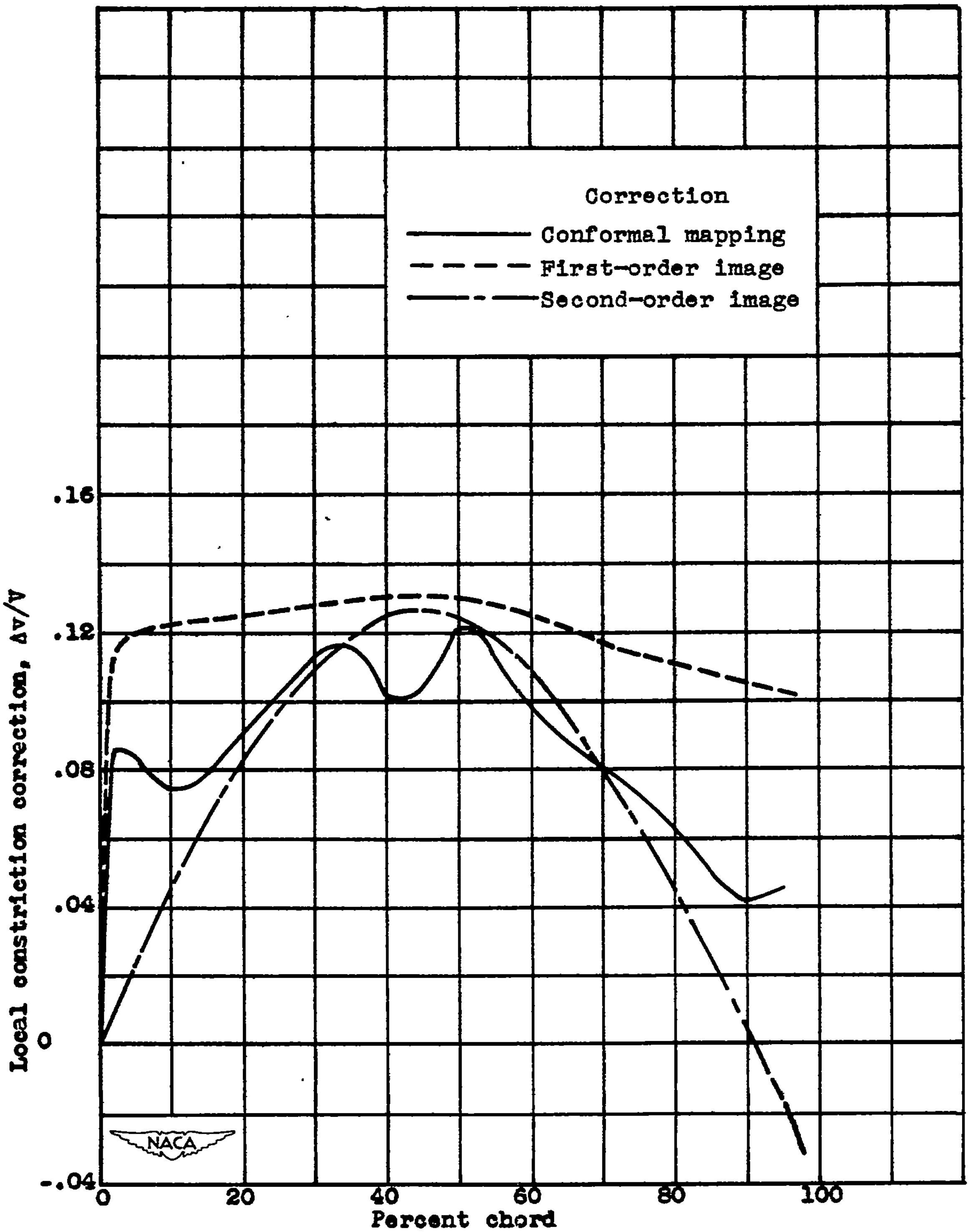

(c) Ratio of chord of airfoil to height of tunnel c/h, 1.5.

Figure 4. - Continued. Local constriction corrections for 12-percent-thick airfoil.

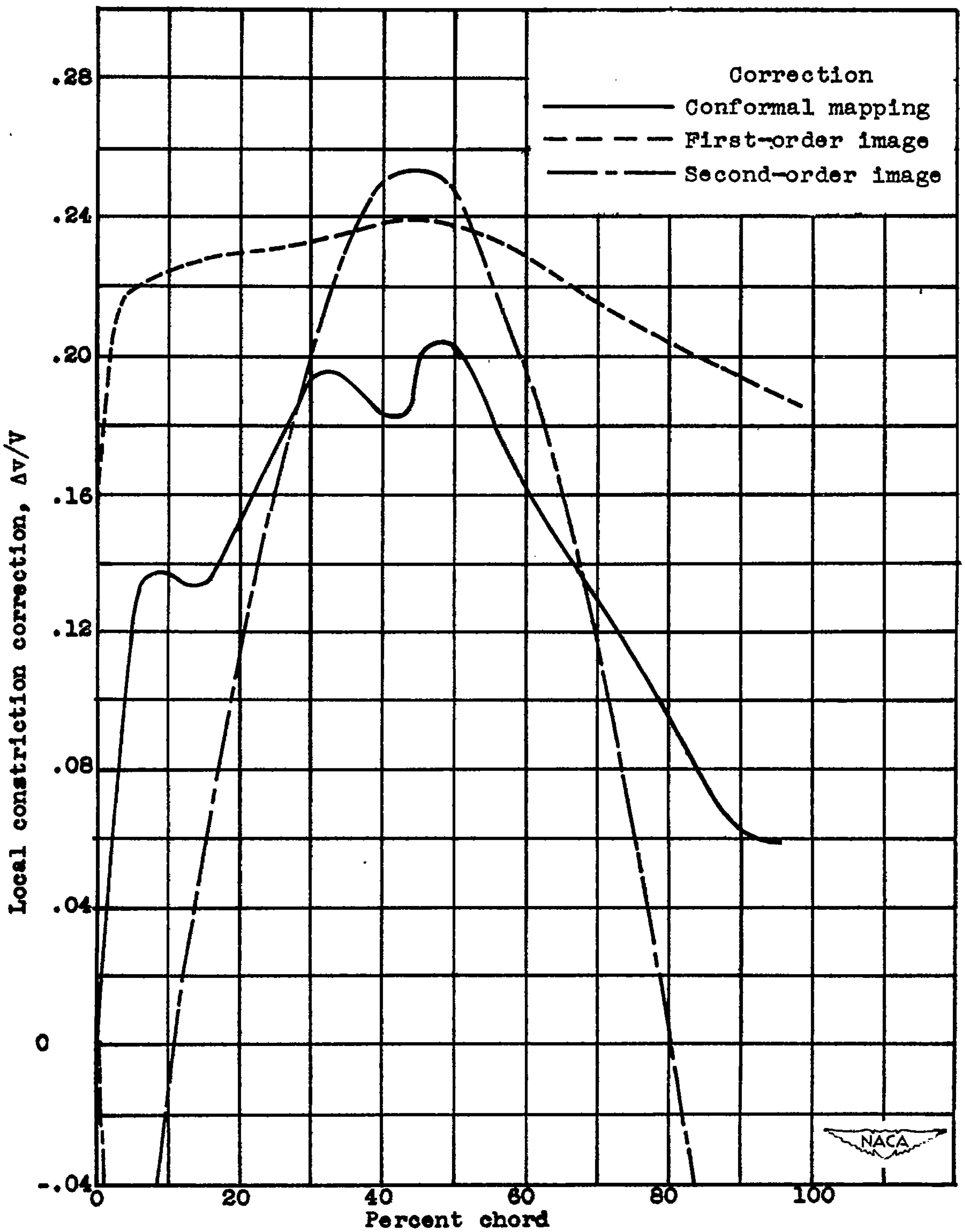

(d) Ratio of chord of airfoil to height of tunnel c/h, 2.0.

Figure 4. - Concluded. Local constriction corrections for 12-percent-thick airfoil.

488

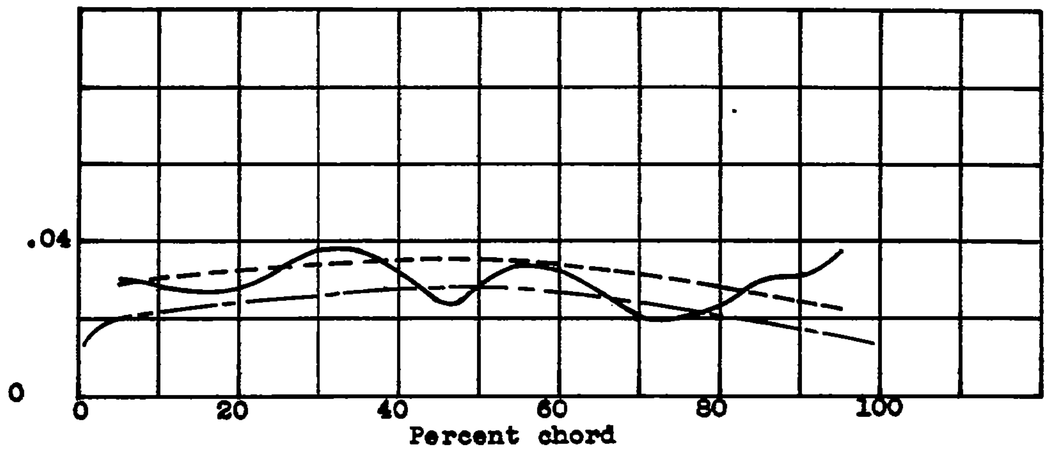

(a) Ratio of chord of airfoil to height of tunnel c/h, 0.5.

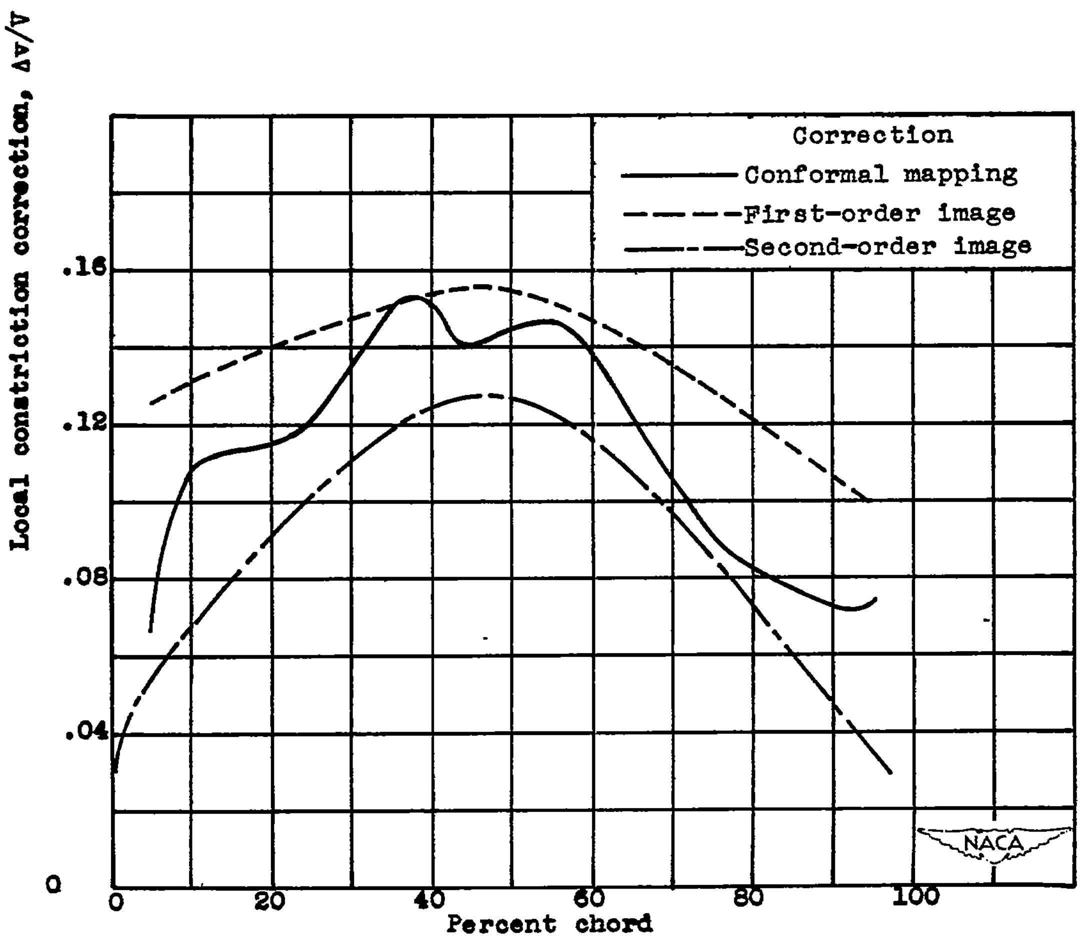

(b) Ratio of chord of airfoil to height of tunnel c/h, 1.0.

Figure 5. - Local constriction corrections for 24-percent-thick airfoil.

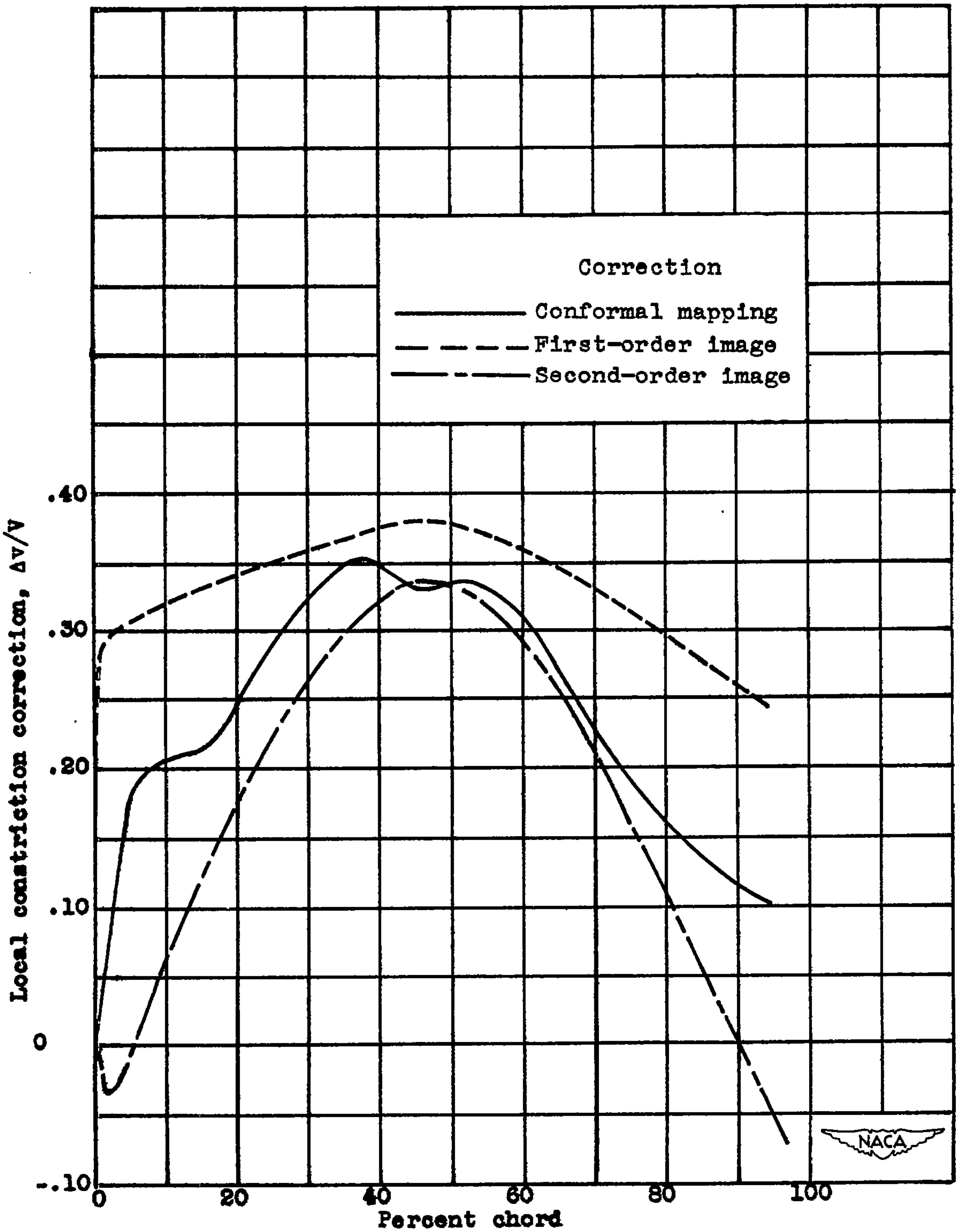

(c) Ratio of chord of airfoil to height of tunnel c/h, 1.5.

Figure 5. - Continued. Local constriction corrections for 24-percent-thick airfoil.

488

488

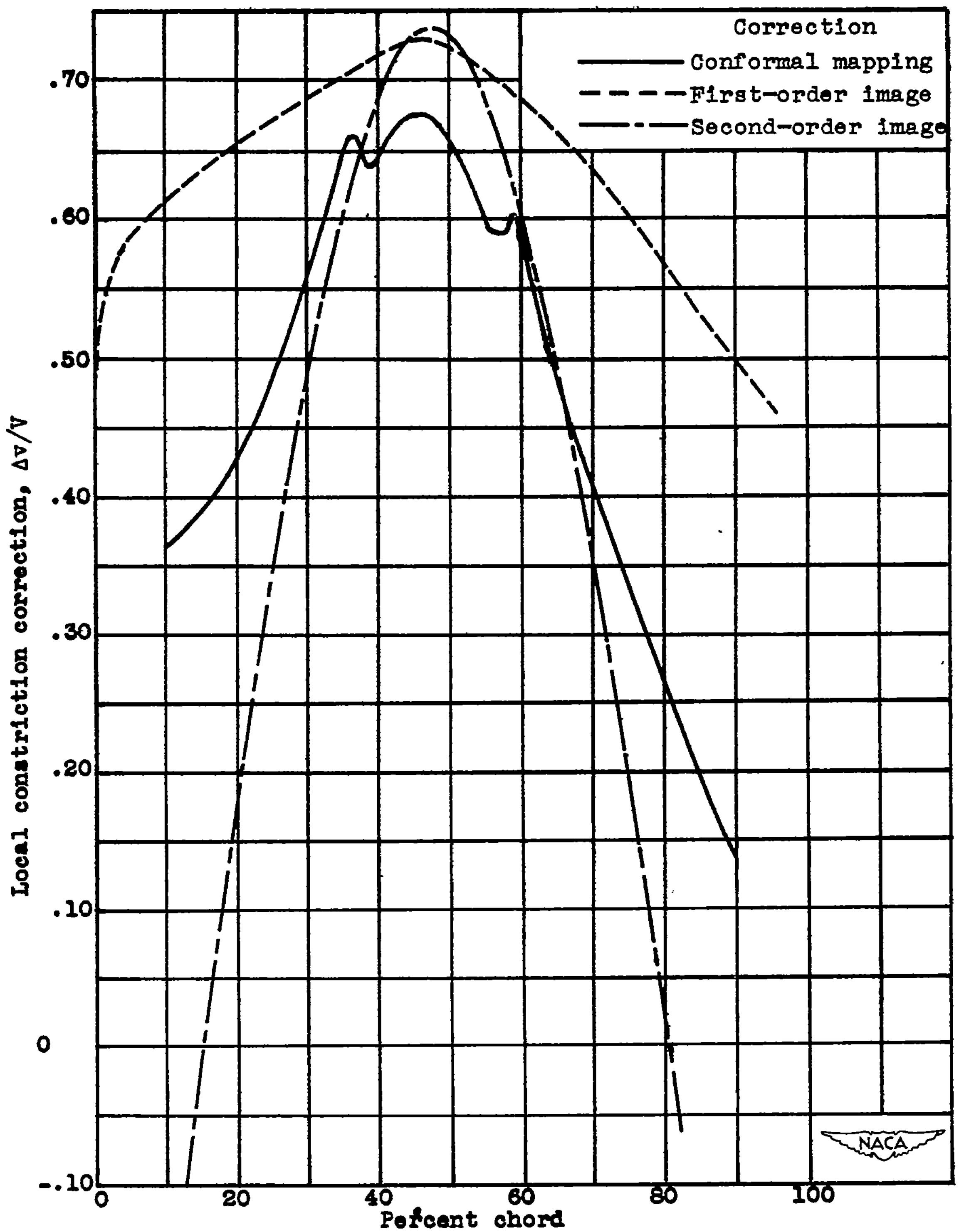

(d) Ratio of chord of airfoil to height of tunnel c/h, 2.0.

Figure 5. - Concluded. Local constriction corrections for 24-percent-thick airfoil.

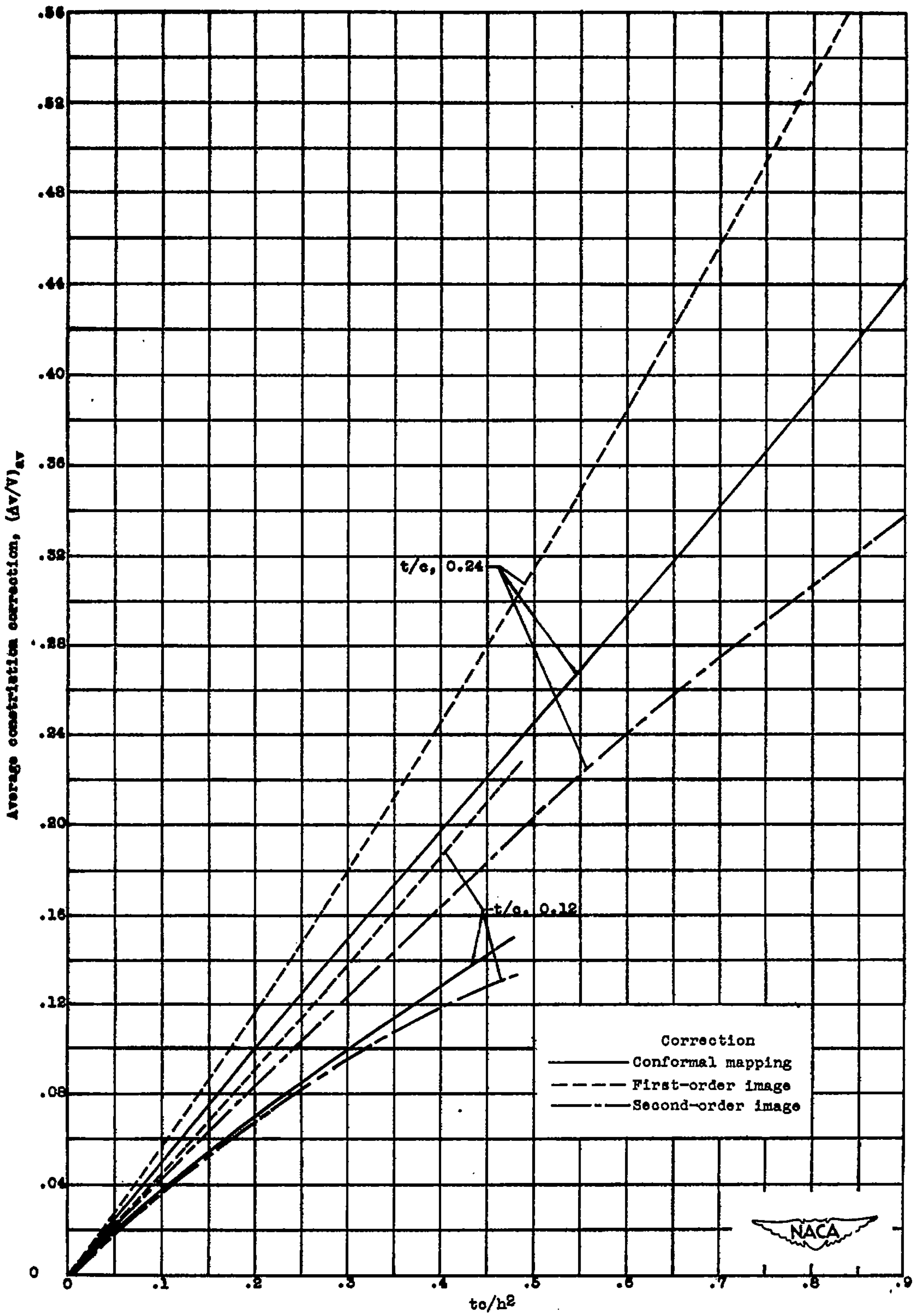

Figure 6.- Comparison of average constriction corrections by different methods. c, chord of airfoil; h, height of tunnel; t, maximum thickness of airfoil.

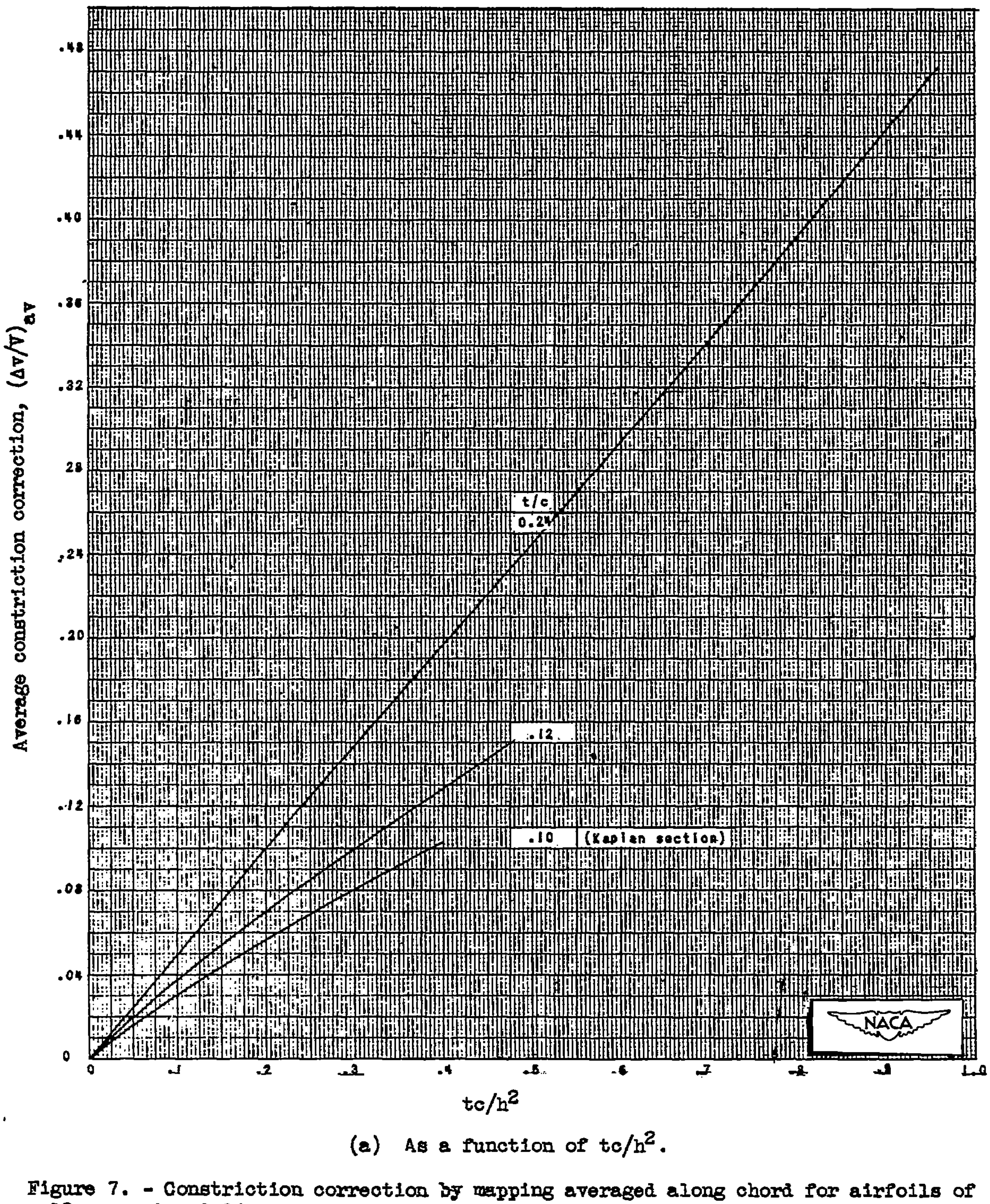

(a) As a function of tc/h^2.

Figure 7. - Constriction correction by mapping averaged along chord for airfoils of 12-percent and 24-percent thickness and a Kaplan section of 10-percent thickness. c, chord of airfoil; h, height of tunnel; t, maximum thickness of airfoil.

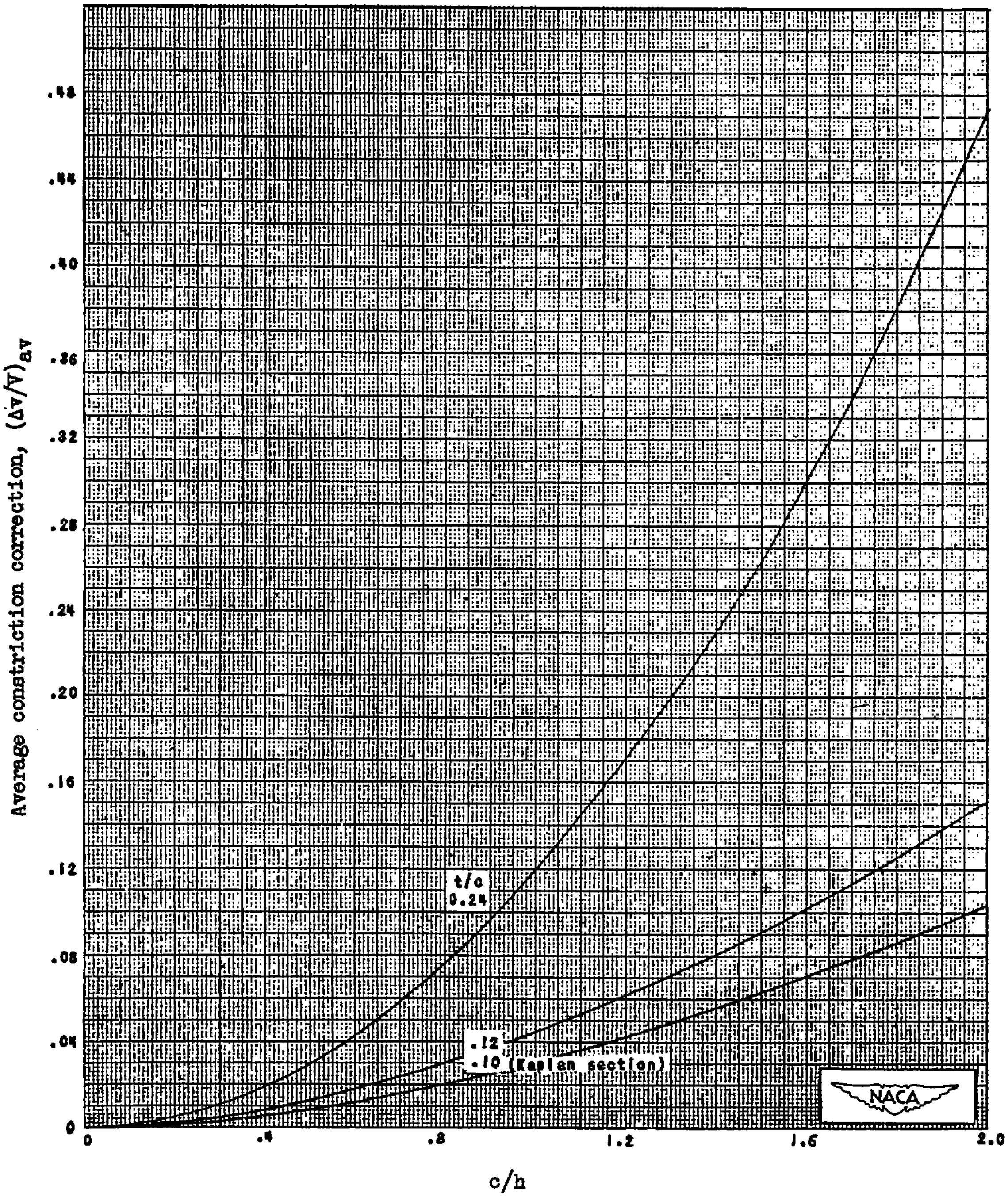

(b) As a function of c/h.

Figure 7. - Continued. Constriction correction by mapping averaged along chord for airfoils of 12-percent and 24-percent thickness and a Kaplan section of 10-percent thickness. c, chord of airfoil; h, height of tunnel; t, maximum thickness of airfoil.

488

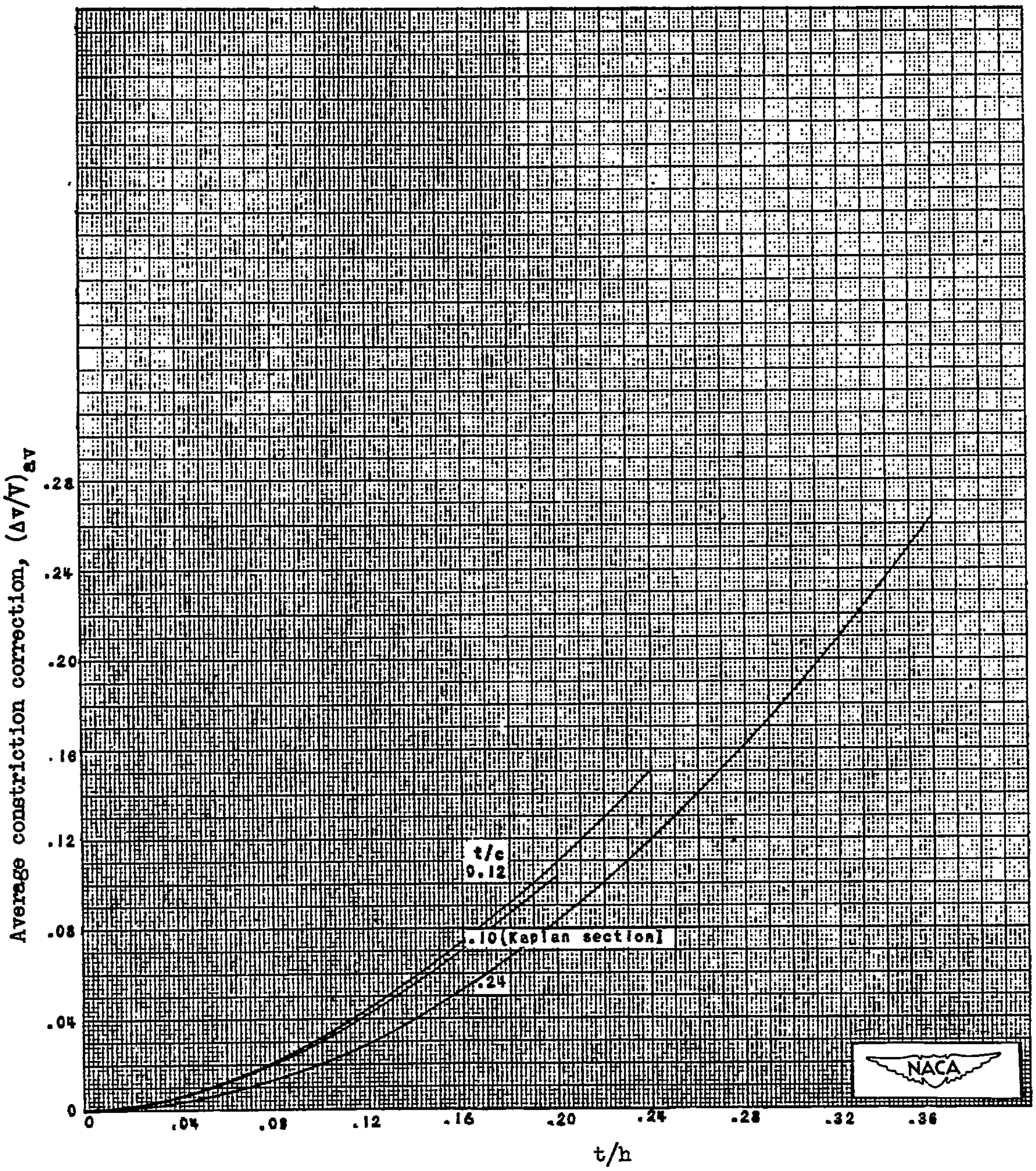

(c) As a function of t/h.

Figure 7. - Concluded. Constriction correction by mapping averaged along chord for airfoils of 12-percent and 24-percent thickness and a Kaplan section of 10-percent thickness. c, chord of airfoil; h, height of tunnel; t, maximum thickness of airfoil.

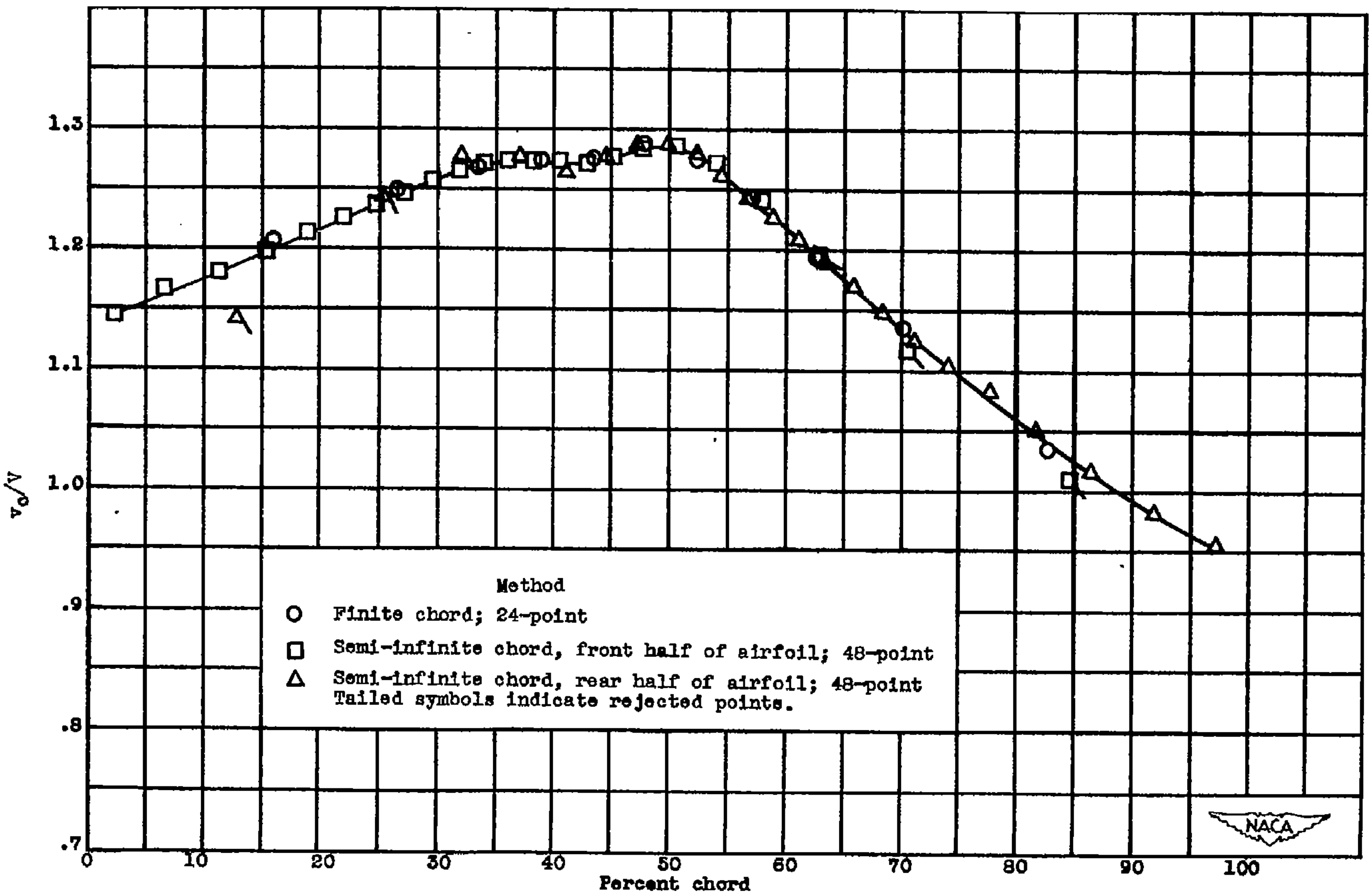

Figure 8. - Comparison of velocity distributions by the two conformal-mapping methods. 12-percent-thick airfoil; $\sigma = 1.5$; v_c, velocity on airfoil in tunnel or equivalent cascades; V, undisturbed stream velocity.